# Surface Acoustic Waves on Piezoelectric Media
## *Applications to Acoustic Charge Transport*

Stuart Hatch
9707918

A dissertation submitted in partial satisfaction
of the requirements for the degree of

Bachelor of Science (Honours)
at the
University of Western Australia

October 2000

Supervisors:

Dr. Robert L. Stamps

Dr. Nick Warrington

# Abstract

Surface acoustic waves are modes of propagation of elastic energy along the surface of a solid, whose displacement amplitudes undergo exponential decay away from this surface. When these waves propagate in piezoelectric material, there is an accompanying electric potential that has the same spatial and temporal periodicities as the surface wave. Acoustic charge transport is a phenomenon that results from the interaction of this potential with a two dimensional electron gas formed within the piezoelectric material, and has been the focus of intensive research in the past five years due the possible optical and quantum computing device applications it presents. This theoretical project has investigated surface acoustic wave propagation for arbitrary directions on the (001) plane of $Al_x\,Ga_{1-x}\,As$. The allowed velocities, decay constants, displacement amplitudes and associated piezoelectric fields and potential have been numerically calculated for these directions. Phonon focusing effects and the variation of the piezoelectric fields and potential at different depths have also been investigated. Based on these results, new suggestions for experimental investigations have been made that minimise Stark effects in the two dimensional electron gas and maximise the piezoelectric potential of the surface acoustic wave.

# Acknowledgements

First and foremost, I would like to thank Dr. Bob Stamps for his continual guidance and encouragement throughout the year. He has provided great enthusiam and remarkable insight toward this project, for which I incredibly grateful.

Thanks also goes to Dr. Nick Warrington and Dr. Paul Abbott for their assistance, and Joo-Von Kim and the Theory crew, whose support and advice throughout the year has been invaluable and very much appreciated. In addition, I would like to acknowledge the Honours class of 2000 and express my sincere appreciation for their helpful encouragement and support throughout this year.

Finally, my heartfelt thanks goes to my family. Without their understanding, patience and support none of this would have never been possible.

# Table of Contents

# Chapter One: Introduction

## 1.1 Surface Acoustic Waves

Research into surface acoustic waves started back in 1887 when Lord Rayleigh first proposed[1] their existence. Surface acoustic waves, (SAW) are modes of propagation of elastic energy along the surface of a solid, whose displacement amplitudes undergo exponential decay beneath this surface. Typically almost all of the energy is localised within a depth of two wavelengths.

Interest in surface acoustic waves has grown since Rayleigh's discovery. They first attracted the attention of seismologists, and continue to, for two reasons: First because of the guided nature of the trajectory of such waves along the earth's surface, and second due to the comparison between these surface waves and bulk waves produced by a disturbance; or, as Lord Rayleigh put it, "diverging in two dimensions only, they must acquire at a great distance from the source a continually increasing preponderance". Over a hundred years after his discovery, there has been a resurgence of studies in surface acoustic waves from condensed matter physicists, interested in acoustic charge transport in piezoelectric semiconductors.

Rayleigh's treatment only involved isotropic media, and the first anisotropic analysis of surface acoustic waves was made by Stoneley[2] in 1955. He produced expressions for propagation in the high symmetry directions on the basal plane of cubic crystals, but failed to recognise a whole set of solutions now known as generalised Rayleigh waves.[3] These solutions, which will be spoken of in depth in chapter two, are characterised by an oscillatory decay away from the free surface, as opposed to the simple exponential decay occurring in isotropic media. Stoneley's neglect of these solutions lead him to the conclusion that surface wave propagation could only exist in a very limited class of cubic crystals.

Studying a more general set of propagation directions on anisotropic media became practical after the advent of high-speed digital computers. Such research[4–6] conducted in the early to mid 1960s on a variety of planes of cubic crystals came to the conclusion that there exists a region of forbidden propagation directions. It was shown[7] later that such regions do not exist, but rather a degeneration of surface modes into bulk modes occur in these directions. This phenomena will also be discussed in chapter two.

The many device applications utilising ultrasonics lead to a resurgence of interest in surface acoustic waves in the late 1960s, including ultrasonic detection of surface flaws[8] and ultrasonic delay lines .[9] Early transducer devices utilising SAWs on piezoelectric crystals[10] emerged around the same time, whilst theoretical considerations of the surface wave problem to include piezoelectric effects was first studied by Tseng.[11,12] Further interest resulted from the multitude of signal

processing applications available utilising surface acoustic waves - partly because the character of the wave can be changed in transit,[13] as well as the fact the wave can be guided[14,15] and even amplified.[13] Ultrasonic amplification was the first phenomena studied that involved interactions with electrons, and the basic theory is outlined in the appendix. This ability to manipulate the surface wave opened up the prospect of creating analogs of the entire line of electromagnetic waveguide devices in elastic media,[16] thereby reducing the size of such a device corresponding to the ratio of the velocity of acoustic waves to electromagnetic waves.

## 1.2 Acoustic Charge Transport

Probably the most interesting application of surface acoustic waves is a phenomenon known as acoustic charge transport (ACT). Acoustic charge transport involves the interaction between surface acoustic waves and free electrons within a piezoelectric semiconductor. Extensive theoretical[17–20] and experimental[21–23] research has been made of late, particularly in the ACT properties of a two-dimensional electron gas (2DEG), formed within a $GaAs/Al_x Ga_{1-x} As$ heterostructure.

A surface acoustic wave propagating upon a piezoelectric crystal has associated with it an electric potential having the same temporal and spatial periodicities as the SAW. This surface wave interacts with the electron gas whereby the electrons are confined within the moving quantum wells formed by the potential. The result is an acoustoelectric current,[24–28] and an attenuation[17–19] of the acoustic wave.

This acoustoelectric current has metrology applications. At present many-junction electron pumps[29] are used as a current standard, which transfer electrons with an error of approximately one part per $10^8$. A drawback of these devices is the low current delivered - of the order of 1pA. Alternatively, the acoustoelectric current is of the order of nanoamps, with comparable error. To direct the current in the $GaAs/Al_x Ga_{1-x} As$ heterostructure, a channel is formed using the split – gate technique,[30] and as a result the acoustoelectric current measured as a function of gate voltage is observed to display a plateau-like structure. The value of the current, $I$, on each plateau is $I = e\,f\,n$, where $e$ is the electron charge, $f$ is the frequency of the SAW and $n$ is the number of electrons transferred through the cycle per cycle. This reflects the number of electrons trapped within the dynamic quantum wells associated with the surface acoustic wave.

Another branch of applications of ACT is the whole new range of acousto-optic devices that can employ this phenomena. As the scale of transistors on silicon based computer chips is approaching the quantum limit, new avenues of computing will have to be followed, one of which is the optical regime. One present technical problem lies in the memory component of such computers. How is light stored? One possibility[31] may follow from the research of Rocke et al,[21] published in Physical Review Letters, eloquently named "Acoustically Driven Storage of Light in a Quantum Well". Optically excited electron-hole pairs, known as excitons, are trapped within

the moving potential associated with the surface acoustic wave. The resulting separation of these electron-hole pairs leads to an increase of the radiative lifetime by orders of magnitude as compared to the unperturbed pairs. External screening of the lateral piezoelectric fields triggers radiative recombination after very long storage times at a remote location on the crystal. (see Fig. 1.1) This conversion of photons into long lived electron-hole pairs which is efficiently reconverted back into photons can serve as an optical delay line, operating at sound velocities.

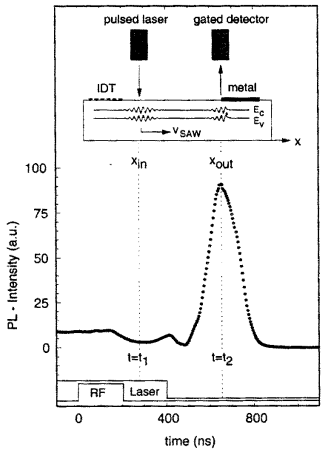


Figure 2.1: The detected photoluminescence (PL) at the gated detector. Optically excited electron-hole pairs are trapped in the moving potential associated with the SAW. This potential is then screened at $x = x_{out}$ by semitransparent metal gates, and the electron-hole pair undergo radiative recombination, as detected at $t = t_2$. [From Rocke et al[21] ]

A significant recent application was proposed[32] in September 2000 for the utilisation of acoustic charge transport phenomena to implement qubits and quantum logic gates of a quantum computer.

# 1.3 Focus of Research

The acoustic charge transport problem requires a deep understanding of the elastic and piezoelectric properties of surface acoustic waves. Although the high symmetry directions of propagation for piezoelectric crystals have been studied extensively ,[11,12] no information could be found on the nature of the piezoelectric potential and associated fields as functions of depth and propagation direction. These two parameters, the propagation direction and depth are the most significant in the design of ACT experiments. The purpose of this project was to investigate how they govern the nature of the piezoelectric potential that mediates the charge transport.

Surface acoustic wave propagation on the (001) plane of the semiconductor alloy $Al_{0.3}$ $Ga_{0.7}$ As is investigated here for arbitrary directions. This is achieved by solving a continuum model of the wave equation wave on an infinite, unbounded half space subject to stress free boundary conditions at the surface, and the requirement that the amplitudes of the solutions vanish at a finite depth below this surface. Piezoelectricity also introduces an additional boundary that requires the continuity of the normal component of the electric displacement across this surface.

The anisotropic nature of the cubic crystal $Al_{0.3}$ $Ga_{0.7}$ As manifests an angular dependence upon all the characteristic properties associated with piezoelectric elastic wave propagation on a free surface. The properties, including allowed velocities, decay constants, associated amplitudes and piezoelectric potential are all numerically determined and investigated in detail for propagation directions between [100] and [110] . This covers all unique directions on the (001) plane (and equivalent planes) for cubic crystals.

The solution to the wave equation is a superposition of three (or four in the case of piezoelectric coupling) plane waves, each with an associated decay constants, which is the component of the wavevector normal to the surface. The nature of these decay constants governs the behaviour of the surface wave below the surface - and provides explanations for the degeneration of surface wave solutions in particular ranges of propagation directions.

The amplitudes of the surface waves are also the focus of attention, and the associated polarisations in a given direction give further information into the piezoelectric coupling. Three polarisations are considered - the vertical component; the longitudinal component, measured along the propagation direction; and the transverse component, measured perpendicular to the sagittal plane, defined as the plane parallel to the surface and normal to the wavevector. Fig. 1.2 shows a surface wave polarised in the sagittal plane, on an isotropic material.

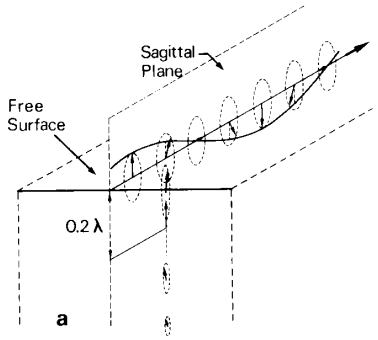


Figure 2.2: The particle displacements for a surface acoustic wave polarised in the sagittal plane in an isotropic material. Particles undergo circular displacements in this plane and the wave has decayed significantly at a depth of 0.2λ [From Dieulesaint and Royer[33] ]

Acoustic charge transport is the result of an electric potential coupled to an acoustic wave, so the most important aspect of the surface wave problem is the piezoelectric potential. This is compared in all directions of propagation and a variety of depths, as are the associated fields. Considerations are also made for phonon focusing effects, which involve the concentration of the flow of energy in particular directions of the crystal. Such effects could have significant upon the nature of the electric fields and potential in particular directions.

The theory behind acoustic charge transport phenomena is discussed in detail. Based on calculations made for the electric potential, suggestions are made of possible combinations of propagation direction and depth of the two dimensional electron gas that would be suitable for acoustic charge transport experiments, and any advantages or disadvantages in doing so. A solution of the Schrödinger equation is derived for an electron travelling through the 2DEG layer within the periodic surface wave potential, and an expression for the energies of these solutions is presented.

The method used and results obtained for non-piezoelectric surface acoustic waves is featured in chapter two, and for piezoelectric SAWs in chapter three, along with an extensive treatment of the piezoelectric fields and potential. Acoustic charge transport and phonon focusing is discussed in chapter four, and chapter five presents a summary of this work and outlines possible future research.

# Chapter Two: Surface Acoustic Waves

Surface acoustic waves are modes of elastic energy propagation governed by the elastic wave equation and boundary conditions that specify a stress free surface. The first section of this chapter presents a general formulation of this problem, which includes the requirement that distinguishes bulk modes of propagation to surface modes - that the associated amplitude of the SAW vanishes in the direction normal to the surface at a finite depth.

In three dimensions, there are three wave equations and three boundary conditions, which can both be formulated into matrix form. The requirement of a vanishing determinant of these matrices is used to determine the wavevectors and the allowed phase velocities, respectively. Furthermore, the boundary condition matrix provides three homogenous equations involving the amplitudes, and when solved in conjunction with the three wave equations, a complete form of the surface wave solution can be established.

## 2.1 Theory and Method

### 2.1.1 Crystal Structure of $Al_x\ Ga_{1-x}\ As$

The III-IV compound alloy $Al_x\ Ga_{1-x}\ As$ has a zinc-blende structure which is based on the cubic space group $\overline{4}3m$. It consists of two interpenetrating face centred cubic sublattices. One sublattice is displaced by 1/4 of a lattice parameter in each direction from the other sublattice, so that each site of one sublattice is tetrahedrally coordinated with sites from the other sublattice. That is, each atom is at the center of a regular tetrahedron forms by four atoms of the opposite type. When the two sublattices have the same type of atom, the zinc-blende lattice becomes the diamond lattice.

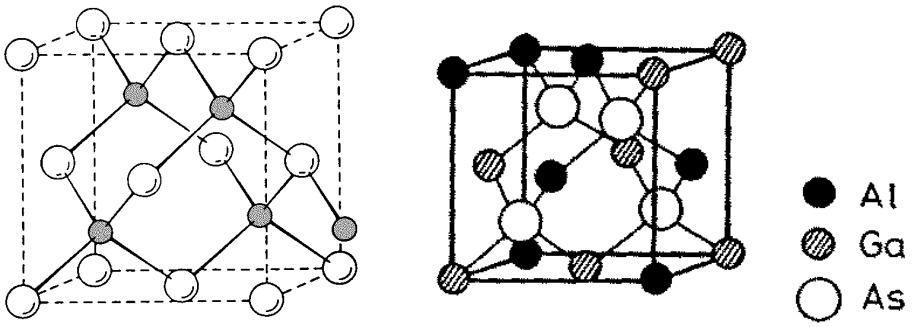


Figure 2.1: The general Zinc-blende cubic crystal structure (left), and the corresponding structure of the alloy $Al_{0.5}$ $Ga_{0.5}$ As (right) [both from Adachi[39]]

The space group $\overline{4}3m$ is characterised by three four fold axes, with inversion; four three fold axes, and six mirror planes. The zinc-blende crystal structure is shown in Fig. 2.1 as well as a specific example of $Al_x$ $Ga_{1-x}$ As with $x = 0.5$. If the three direct two fold axes are chosen as the reference frame, it can be shown[33] that the non vanishing components of the elastic moduli tensor for a crystal with cubic symmetry becomes:

$$(c_{\alpha\beta}) = \begin{vmatrix} c_{11} & c_{12} & c_{12} & 0 & 0 & 0 \\ c_{12} & c_{11} & c_{12} & 0 & 0 & 0 \\ c_{12} & c_{12} & c_{11} & 0 & 0 & 0 \\ 0 & 0 & 0 & c_{44} & 0 & 0 \\ 0 & 0 & 0 & 0 & c_{44} & 0 \\ 0 & 0 & 0 & 0 & 0 & c_{44} \end{vmatrix} \tag{2.1}$$

with three independent elastic constants, $c_{11}$, $c_{12}$, and $c_{44}$. The values for each of the elastic constants and the density for the $Al_x$ $Ga_{1-x}$ As alloy depend linearly[38] upon the aluminium concentration ratio $x$. For $Al_{0.3}$ $Ga_{0.7}$ As, the values of the elastic constants are:

$$\begin{aligned} c_{11} &= 11.922 \times 10^{10}\ \mathrm{Nm}^{-2} \\ c_{12} &= 5.476 \times 10^{10}\ \mathrm{Nm}^{-2} \\ c_{44} &= 5.925 \times 10^{10}\ \mathrm{Nm}^{-2} \\ \rho &= 4.88 \times 10^{3}\ \mathrm{kgm}^{-3} \end{aligned}$$

### 2.1.2 Geometry of system

The model geometry for acoustic charge transport experiments is represented in Fig. 2.2. A satisfactory approximation when solving for surface wave modes is an infinite half space $z \leq 0$ unbounded in the x and y direction. Surface waves are localised in the xy plane, and their amplitudes decay into the bulk of the medium; as $z \to -\infty$. The cartesian axes are aligned to the crystal axes whereby wave propagation occurs on the (001) plane of $Al_x\ Ga_{1-x}$ As.

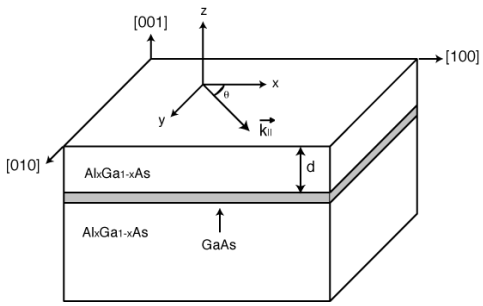


Figure 2.2: Approximate model geometry for acoustic charge transport experiments.

The two dimensional electron gas forms within the GaAs layer, which is located at a distance d from the surface, usually on the order of $100 - 500$ nm. The layer is considered here as an infinitesmal slab, and thus interface effects between the $Al_x\ Ga_{1-x}$ As and GaAs can be neglected. This approximation holds as the GaAs layer is on the order of 10nm, and the lattice constants and elastic constants of the two media are very similar.

### 2.1.3 The Wave Equation

In the absence of external forces, the wave equation for a perfectly elastic, homogeneous, anisotropic medium can be written as

$$\rho \frac{\partial^2 u_i}{\partial t^2} = \frac{\partial T_{\mathrm{ij}}}{\partial x_j}$$

where $u_i$ are the displacements measured along the three cartesian axes $x_i$ ($x_1 = x,\ x_2 = y,\ x_3 = z$). The density of the medium is $\rho$, and the stress tensor, $T_{\mathrm{ij}}$, neglecting piezoelectric effects is defined as in appendix A.2 (Eqn. 0.22):

$$T_{\mathrm{ij}} = c_{\mathrm{ijkl}} \frac{\partial u_l}{\partial x_k}$$

With summation implied over the repeated indicies, the wave equation in full looks like:

$$\rho \frac{\partial^2 u_i}{\partial t^2} = c_{\text{ijkl}} \frac{\partial u_l}{\partial x_j \partial x_k} \tag{2.2}$$

In the case of a crystal with cubic symmetry, the elastic stiffness tensor $c_{\text{ijkl}}$ has three independent elastic constants, $c_{11}$, $c_{12}$ and $c_{44}$. For the three orthogonal displacements $u_x$, $u_y$ and $u_z$, the wave equation breaks into three partial wave equations. Taking the cubic symmetry into account, they are:

$$\begin{aligned}
\rho \frac{\partial^2 u_x}{\partial t^2} &= c_{11} \frac{\partial^2 u_x}{\partial x^2} + c_{44}\left(\frac{\partial^2 u_x}{\partial y^2} + \frac{\partial^2 u_x}{\partial z^2}\right) + (c_{12} + c_{44})\left(\frac{\partial^2 u_y}{\partial x \partial y} + \frac{\partial^2 u_z}{\partial x \partial z}\right) \\
\rho \frac{\partial^2 u_y}{\partial t^2} &= c_{11} \frac{\partial^2 u_y}{\partial y^2} + c_{44}\left(\frac{\partial^2 u_y}{\partial x^2} + \frac{\partial^2 u_y}{\partial z^2}\right) + (c_{12} + c_{44})\left(\frac{\partial^2 u_x}{\partial x \partial y} + \frac{\partial^2 u_z}{\partial y \partial z}\right) \\
\rho \frac{\partial^2 u_z}{\partial t^2} &= c_{11} \frac{\partial^2 u_z}{\partial z^2} + c_{44}\left(\frac{\partial^2 u_z}{\partial x^2} + \frac{\partial^2 u_z}{\partial y^2}\right) + (c_{12} + c_{44})\left(\frac{\partial^2 u_x}{\partial x \partial z} + \frac{\partial^2 u_y}{\partial y \partial z}\right)
\end{aligned} \tag{2.3}$$

Assuming plane waves solutions $u_i$, with wavevector $\mathbf{k} = (k_x, k_y, k_z)$, frequency $\omega$ and amplitude of displacement $A_i$ with the form:

$$u_i = A_i \, \text{Exp}[i\,(k_x\, x + k_y\, y + k_z\, z - \omega\, t)]$$

The differential operators expressed in the partial wave equations (Eqn. 2.3) can be written in terms of wavenumbers and frequencies:

$$\frac{\partial}{\partial x} \equiv i\, k_x \qquad \frac{\partial}{\partial y} \equiv i\, k_y \qquad \frac{\partial}{\partial z} \equiv i\, k_z \qquad \frac{\partial}{\partial t} \equiv -i\, \omega \tag{2.4}$$

The plane wave solution can be used to express to most general solution of the wave equation free of boundary conditions. Such elastic waves that propagate in an unbounded medium are know as bulk waves. When dealing with surface waves is it useful to consider a wavevector parallel to the surface, defined as $k_{||}$, where

$$\boldsymbol{k}_{||} = k_x\, \hat{x} + k_y\, \hat{y}$$

So now the plane wave solution can be a function of direction upon the surface by redefining the wavenumbers as

$$\frac{k_x}{k_{||}} = \text{Cos}(\theta) \qquad \frac{k_y}{k_{||}} = \text{Sin}(\theta) \qquad \frac{k_z}{k_{||}} = \kappa$$

where $\theta$ is the angle between the x-axis and $k_{||}$. The wavenumber in the z-direction is characterised by a decay constant, $\kappa$. The plane wave solutions are now of the form:

$$u_i = A_i \, \mathrm{Exp}[i\, k_{||}\, \kappa\, z] \, \mathrm{Exp}[i\, k_{||} (\mathrm{Cos}(\theta)\, x + \mathrm{Sin}(\theta)\, y - V\, t)] \tag{2.5}$$

where V is the phase velocity of the SAW defined as V = $\frac{\omega}{k_{||}}$. Substituting these into the partial waves equations (Eqn. 2.3) transformed by Eqn. 2.4, a 3×3 matrix, $\mathcal{M}$, can be formed:

$$\mathcal{M} = \begin{pmatrix} c_{11}\,\mathrm{Cos}(\theta)^2 + c_{44}(\mathrm{Sin}(\theta)^2 + \kappa^2) - \rho V^2 & (c_{12} + c_{44})\,\mathrm{Cos}(\theta)\,\mathrm{Sin}(\theta) & (c_{12} + c_{44})\,\mathrm{Cos}(\theta) \\ (c_{12} + c_{44})\,\mathrm{Cos}(\theta)\,\mathrm{Sin}(\theta) & c_{11}\,\mathrm{Sin}(\theta)^2 + c_{44}(\mathrm{Cos}(\theta)^2 + \kappa^2) - \rho V^2 & (c_{12} + c_{44})\,\mathrm{Sin}(\theta) \\ (c_{12} + c_{44})\,\mathrm{Cos}(\theta)\,\kappa & (c_{12} + c_{44})\,\mathrm{Sin}(\theta)\,\kappa & c_{11}\,\kappa^2 + c_{44} - \rho V \end{pmatrix}$$

where

$$\mathcal{M}.\begin{pmatrix} A_x \\ A_y \\ A_z \end{pmatrix} = \begin{pmatrix} 0 \\ 0 \\ 0 \end{pmatrix} \tag{2.6}$$

### 2.1.4 Surface Wave Solutions

Surface waves of the form given in Eqn. 2.5 are defined such that the quantity $\kappa$ must be lead to the amplitudes of displacement to vanish as $z \to -\infty$. This requires $\kappa$ to have a negative imaginary component. In this respect, the z-dependence of Eqn. 2.5 is regarded as part of the amplitude, and the wavelike properties are

$$\mathrm{Exp}[i\, k_{||}(\mathrm{Cos}(\theta)\, x + \mathrm{Sin}(\theta)\, y - V\, t)]$$

So, if $\kappa$ is complex rather than purely imaginary, the wavevector is still assumed to be parallel to the surface. Similarly, the planes of constant phase are perpendicular to the sagittal plane. The amplitude varies in the z-direction over a plane of constant phase according to the real component of the decay constant.

For a non trivial solutions of the three homogeneous equations (Eqn. 2.6), the determinant of $\mathcal{M}$ must vanish, ie:

$$|\mathcal{M}| = 0 \tag{2.7}$$

This is known as the secular equation and is a sixth order equation in $\kappa$ with phase velocity V and propagation direction $\theta$ as parameters. As the coefficients of the powers of $\kappa$ in Eqn. 3.9 are all real, there will be, in general, three complex-conjugate roots. The roots lying in the upper half of the complex plane will lead to a solution (Eqn. 2.5) that will exponentially increase to infinity as $z \to -\infty$. For a surface wave solution, these three roots are disregarded as they do not satisfy the condition that the displacements vanish into the bulk of the medium. The other three roots

$$\kappa_r \equiv \kappa_r(V, \theta) \qquad r = 1, 2, 3$$

are chosen, which give solutions that correspond to surface waves. The phase velocity is the same for each $\kappa_r$ and is determined from the boundary conditions, as discussed later. A linear combination of the solution given in Eqn. 2.5 for each $\kappa_r$ now forms the assumed solution for a surface acoustic wave, which reads

$$u_i = \sum_{r=1}^{3} A_{i,r}\, \mathrm{Exp}[i\, k_{\|}\, \kappa_r\, z]\, \mathrm{Exp}[i\, k_{\|}(\mathrm{Cos}(\theta)\, x + \mathrm{Sin}(\theta)\, y - V\, t)] \tag{2.8}$$

Notice now for each chosen root of the secular equation $\kappa_r$ there exists an associated amplitude $A_{i,r}$. For each displacement $u_i$ there are three amplitudes components to be determined, so a total of nine amplitudes have to be found.

### 2.1.5 Boundary Conditions

As the medium, in the half space $z < 0$, is unbounded in the x and y direction, the elastic boundary conditions are such that the surface $z = 0$ is stress free; ie, no external forces are acting upon it. From the definition of stress from section 2.1.3:

$$T_{\mathrm{ij}} = c_{\mathrm{ijkl}}\, \frac{\partial u_l}{\partial x_k}$$

The stress free condition can be expressed as:

$$T_{\mathrm{i3}} = c_{\mathrm{i3kl}}\, \frac{\partial u_l}{\partial x_k} = 0 \quad at \quad z = 0 \tag{2.9}$$

So, in other words, for the boundary condition to be satisfied, it is required that:

$$T_{13} = T_{23} = T_{33} = 0 \quad at \quad z = 0$$

Using Eqn. 2.9 and the same assumptions from Eqn. 2.4, stresses at the surface $z = 0$ become

$$T_{13} = c_{44}\left(\frac{\partial u_z}{\partial x} + \frac{\partial u_x}{\partial z}\right) = -i\, c_{44}(\, k_x\, u_z + k_z\, u_x) = 0 \qquad at \quad z = 0$$

$$T_{23} = c_{44}\left(\frac{\partial u_z}{\partial y} + \frac{\partial u_y}{\partial z}\right) = -i\, c_{44}(k_y\, u_z + k_z\, u_y) = 0 \qquad at \quad z = 0$$

$$T_{33} = c_{12}\left(\frac{\partial u_x}{\partial x} + \frac{\partial u_y}{\partial y}\right) + c_{11}\, \frac{\partial u_z}{\partial z} =$$

$$-i\, c_{12}(k_x\, u_x + k_y\, u_y) - i\, c_{11}\, k_z\, u_z = 0 \qquad at \quad z = 0$$

Simplifying and constructing the superposition by summing over each $\kappa_r$, the final form of the three boundary conditions are

$$\sum_{r=1}^{3} (c_{44}\,\mathrm{Cos}(\theta)\,A_{z,r} + c_{44}\,\kappa_r\,A_{x,r}) = 0$$

$$\sum_{r=1}^{3} (c_{44}\,\mathrm{Sin}(\theta)\,A_{z,r} + c_{44}\,\kappa_r\,A_{y,r}) = 0 \qquad (2.10)$$

$$\sum_{r=1}^{3} (c_{12}\,\mathrm{Cos}(\theta)\,A_{x,r} + c_{12}\,\mathrm{Sin}(\theta)\,A_{y,r} + c_{11}\,\kappa_r\,A_{z,r}) = 0$$

### 2.1.6 Amplitudes

The superposition solution (Eqn. 2.8) leads to a system with nine unknowns $A_{i,r}$ and six equations from the three wave equations and the three boundary conditions. By considering the three wave equations (Eqn. 2.6) and dividing through by one of the amplitudes, say $A_{z,r}$;

$$\begin{aligned}
&\cos(\theta)\sin(\theta)\,(c_{12}+c_{44})\,\mathcal{Y}_r + \cos(\theta)\,(c_{12}+c_{44})\,\kappa_r + \\
&\quad \mathcal{X}_r\,(\cos^2(\theta)\,c_{11} - \rho\,V^2 + c_{44}\,(\sin^2(\theta) + {\kappa_r}^2)) = 0 \\
&c_{11}\,{\kappa_r}^2 - \rho\,V^2 + c_{44} + \cos(\theta)\,(c_{12}+c_{44})\,\mathcal{X}_r\,\kappa_r + \sin(\theta)\,(c_{12}+c_{44})\,\mathcal{Y}_r\,\kappa_r = 0 \\
&\sin(\theta)\,(c_{12}+c_{44})\,\kappa_r + \mathcal{Y}_r\,(-\rho\,V^2 + \sin^2(\theta)\,c_{11} + c_{44}\,(\cos^2(\theta) + {\kappa_r}^2)) = 0
\end{aligned}$$

amplitude ratios can be defined:

$$\mathcal{X}_r \equiv \mathcal{X}_r(V,\theta) = \frac{A_{x,r}}{A_{z,r}} \qquad \textit{and} \qquad \mathcal{Y}_r \equiv \mathcal{Y}_r(V,\theta) = \frac{A_{y,r}}{A_{z,r}}$$

Choosing any two of the above equations and solving will yield explicit expressions for these ratios. These amplitude ratios, being dependent upon the parameters direction and phase velocity contain information on how the polarisation of the surface wave changes as the wavevector is rotated through an angle of $\theta$. But most importantly they can be substituted back into the boundary conditions (Eqn. 2.10) such that each can be expressed by only three amplitude components - in this case $A_{z,r}$:

$$\sum_{r=1}^{3} (c_{44}\,\mathrm{Cos}(\theta)\,A_{z,r} + c_{44}\,\kappa_r\,\mathcal{X}_r\,A_{z,r}) = 0$$

$$\sum_{r=1}^{3} (c_{44}\,\mathrm{Sin}(\theta)\,A_{z,r} + c_{44}\,\kappa_r\,\mathcal{Y}_r\,A_{z,r}) = 0$$

$$\sum_{r=1}^{3} (c_{12}\,\mathrm{Cos}(\theta)\,\mathcal{X}_r\,A_{z,r} + c_{12}\,\mathrm{Sin}(\theta)\,\mathcal{Y}_r\,A_{z,r} + c_{11}\,\kappa_r\,A_{z,r}) = 0$$

Now the boundary conditions contain only the amplitudes $A_{z,r}$, so a 3×3 matrix, $\mathcal{B}$, known as the boundary condition matrix can be formed, where:

$$\mathcal{B}.\begin{pmatrix} A_{z,1} \\ A_{z,2} \\ A_{z,3} \end{pmatrix} = \begin{pmatrix} 0 \\ 0 \\ 0 \end{pmatrix} \tag{2.11}$$

The form of the boundary conditions and thus the boundary condition matrix depends upon the choice of amplitude ratios. This leads to the question whether one choice is better than another. As the direction of propagation along the surface changes, so do the associated amplitudes of the elastic wave. In some particular directions, some polarisations are absent - which is reflected in the fact that one of the components of displacement $u_i$ is zero. This will correspond to a zero amplitude - and thus dividing Eqns. 2.6 by this amplitude will lead to algebraic singularities in such directions within the boundary condition matrix. It is important to ensure that for each direction, the amplitude ratios are finite.

For the set of boundary conditions and amplitude ratios defined above, the $\mathcal{B}$ matrix looks like

$\mathcal{B} =$

$$\begin{pmatrix} \cos(\theta)\,c_{44} + \mathcal{X}_1\,\kappa_1\,c_{44} & \cos(\theta)\,c_{44} + \mathcal{X}_2\,\kappa_2\,c_{44} & \cos(\theta)\,c_{44} + \mathcal{X}_3\,\kappa_3\,c_{44} \\ \sin(\theta)\,c_{44} + \mathcal{Y}_1\,\kappa_1\,c_{44} & \sin(\theta)\,c_{44} + \mathcal{Y}_2\,\kappa_2\,c_{44} & \sin(\theta)\,c_{44} + \mathcal{Y}_3\,\kappa_3\,c_{44} \\ \cos(\theta)\,c_{12}\,\mathcal{X}_1 + \sin(\theta)\,c_{12}\,\mathcal{Y}_1 + c_{11}\,\kappa_1 & \cos(\theta)\,c_{12}\,\mathcal{X}_2 + \sin(\theta)\,c_{12}\,\mathcal{Y}_2 + c_{11}\,\kappa_2 & \cos(\theta)\,c_{12}\,\mathcal{X}_3 + \sin(\theta)\,c_{12}\,\mathcal{Y}_3 + c_{11}\,\kappa_3 \end{pmatrix}$$

For a non trivial solution of Eqn. 2.11 the determinant of $\mathcal{B}$ must vanish. As the amplitudes $A_{z,r}$ can be complex, the determinant is, in general also complex. For any particular choice of V, it is unlikely to give values of the amplitude ratios and $\kappa_r$ such that the real and imaginary parts of the determinant of $\mathcal{B}$ are both zero. The algebraic complexity of this determinant makes it impractical to try and derive an analytical expression for velocity that sees it vanish. Instead it is worth plotting out the real and imaginary parts of $|\mathcal{B}|$ as a function of velocity, and finding the roots by inspection. Many root finding routines, especially those based upon derivatives tend to fail due to the rapid variation of the magnitude of $|\mathcal{B}|$ near the correct velocity, as illustrated in Fig. 2.3. As a consquence, root finding becomes quite tedious.

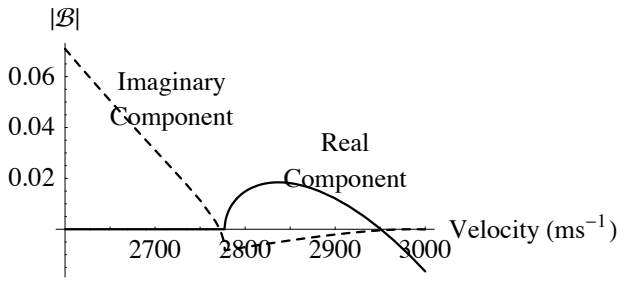


Figure 2.3: The real and imaginary components of the determinant of $\mathcal{B}$ as a function of velocity for $\theta = \frac{\pi}{3}$. The only definite zero lies at $V \simeq 2770\ \mathrm{ms}^{-1}$.

The velocities where the determinant of $\mathcal{B}$ vanish correspond to, for a particular direction of propagation $\theta$, the allowed phase velocities of the surface wave. Once this has been determined, only the amplitudes $A_{i,r}$ remain to be found to completely determine the form of the surface wave as described by Eqn. 2.8. Subsituting the allowed velocity into the amplitude ratios, decay constants and boundary condition matrix gives three boundary condition equations that can be used to solve for these amplitudes.

The homogenous nature of these equations allows only for solutions of two amplitudes in terms of a the third. By dividing through by one of these amplitudes and setting it to unity, a numerical form of each can be specified. Again the choice of which amplitude to divide through becomes important, as in particular directions some amplitudes are zero. Once these three amplitudes are found, the amplitude ratios can be used to find the remaining six amplitudes.

## 2.2 Results and Discussion

Using the method just outlined, extensive analysis of the solutions that correspond to surface acoustic modes for the (001) plane of $Al_{0.3}\,Ga_{0.7}\,As$ are presented in the following section, neglecting piezoelectric effects.

Propagation directions in single degree steps between and including [100] and [110] are considered, which covers all unique SAW solutions for cubic crystals in this plane. These results present the most detailed analysis of surface wave propagation in $Al_x\,Ga_{1-x}\,As$ to date, and they include discussions of:

-allowed velocities and decay constants for SAW modes on the (001) plane;

-the variation of displacement amplitudes;

-the appearance of leaky modes; and
-the degeneration of the SAW mode into a bulk transverse mode.

### 2.2.1 High symmetry directions

*Propagation in the [100] direction*

The wave equation simplifies for high symmetry directions of propagation. Such directions have been the focus of extensive research[33,35] so only a brief discussion will be included here. For a surface wave travelling in the [100] direction ($\theta = 0$ and $k_{||} = k_x$), the wave equation matrix $\mathcal{M}$ looks like

$$\mathcal{M} = \begin{pmatrix} c_{44}\,k^2 - V^2\,\rho + c_{11} & 0 & k\,c_{12} + k\,c_{44} \\ 0 & c_{44}\,k^2 - V^2\,\rho + c_{44} & 0 \\ k\,c_{12} + k\,c_{44} & 0 & c_{11}\,k^2 - V^2\,\rho + c_{44} \end{pmatrix}$$

Notice that in this case, the second row of this matrix contains only one component, and thus $A_y = 0$. Displacements are confined to the sagittal plane and are of the form of a transverse ($A_z$) and a longitudinal ($A_x$) component. The above matrix can be reformed as a 2×2 matrix $\mathcal{M}$, such that

$$\mathcal{M}.\begin{pmatrix} A_x \\ A_z \end{pmatrix} = \begin{pmatrix} 0 \\ 0 \end{pmatrix}$$

Setting the determinant to zero will lead to a quadratic equation in $\kappa$, and the two roots in the lower complex plane are chosen. Each displacement will be a superposition of two terms, rather than three, corresponding to the two roots $\kappa_2$ and $\kappa_3$. Further, only two of the three boundary conditions are required and only one amplitude ratio needs to be defined in order to solve completely for the form of the surface wave.

The requirement of a vanishing determinant of the boundary condition matrix (only a 2×2 in this case) gave the allowed velocity of the surface wave in this direction to be 2830.6 $ms^{-1}$. Fig. 2.4 shows the z-dependence of this Rayleigh wave solution, characterised by an oscillatory decay into the bulk.

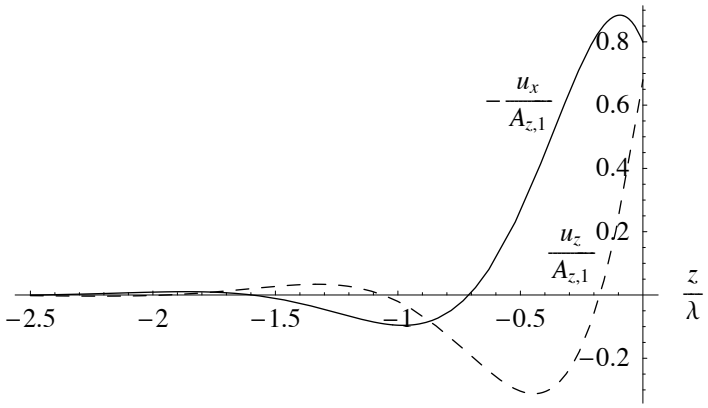


Figure 2.4: The variation of transverse and longitudinal components of a Rayleigh wave propagating in the [100] direction, as a function of depth (in wavelengths).

A very similar solution exists for the propagation direction [010], where $k_{||} = k_y$. In this case, the transverse component $u_x = 0$, and the displacements are confined to the sagittal plane.

### *Propagation in the [110] direction*

It will be shown in section 2.2.3 that in the [110] direction $\kappa_1 = 0$. As a result, the general method of solving for surface waves solutions outlined in the first section of this chapter breaks down at $\theta = 45\,°$. The fact that $\kappa_1 = 0$ would correspond to a plane wave solution which would be invariant in z-direction, and the same displacement caused by this plane wave would exist at the surface and all the way through the bulk. This solution corresponds to a bulk elastic wave. Interestingly enough this bulk mode, polarised perpendicular to the sagittal plane, satisfies the boundary conditions associated with a stress free surface. Although in order to meet the condition of a vanishing displacement below the surface, an alteration to the method of solving for surface waves propagating in the [110] direction is required.

Now that $\kappa_1$ is to be disregarded, all corresponding terms in the superposition involving $\kappa_1$ also need to be disregarded - in the final form of the solution and in the boundary conditions. In both cases, the superposition will only involve two terms, and one of the consequences of this is that the boundary condition matrix now becomes a 2×2 matrix. From the first two boundary conditions for the $\theta = 45\,°$ case:

$$\frac{c_{44}}{\sqrt{2}} A_{z,r} + c_{44}\ \kappa_r\, A_{x,r} = 0$$

$$\frac{c_{44}}{\sqrt{2}} A_{z,r} + c_{44}\, \kappa_r\, A_{y,r} = 0$$

It is obvious that $A_{x,r} = A_{y,r}$; which physically represents a transverse mode of propagation. In the boundary condition matrix, the first column corresponds to terms involving $\kappa_1$, so this is removed. In order to be able to find the allowed velocity of the SAW for this propagation direction, the determinant must vanish - so the matrix needs to be square. The first row is removed - as this contains information on $A_{x,1}$ and $A_{x,2}$, which, as shown above is equal to the $A_y$ components. The boundary condition matrix will look like

$$\mathcal{B} = \begin{pmatrix} \frac{c_{44}}{\sqrt{2}} + \mathcal{Y}_2\, \kappa_2\, c_{44} & \frac{c_{44}}{\sqrt{2}} + \mathcal{Y}_3\, \kappa_3\, c_{44} \\ \frac{c_{12}}{\sqrt{2}} (\mathcal{X}_2 + \mathcal{Y}_2) + c_{11}\, \kappa_2 & \frac{c_{12}}{\sqrt{2}} (\mathcal{X}_3 + \mathcal{Y}_3) + c_{11}\, \kappa_3 \end{pmatrix}$$

The corresponding allowed velocity was found to be $2980.4\,\mathrm{ms}^{-1}$, which is the theoretically accepted velocity in the [110] direction of $Al_{0.3}\,Ga_{0.7}\,As$, as discussed later in this chapter. This fact verifies that the assumption to alter the boundary condition matrix as above was correct.

Surface acoustic waves travelling in this direction have two transverse modes - one parallel to the surface where $u_x = u_y$, and the other perpendicular, $u_z$. The decay constants are $\kappa = \pm 0.483 - 0.498\, i$, and both will contribute to an oscillatory variation of these displacements beneath the free surface, as shown in Fig. 2.5.

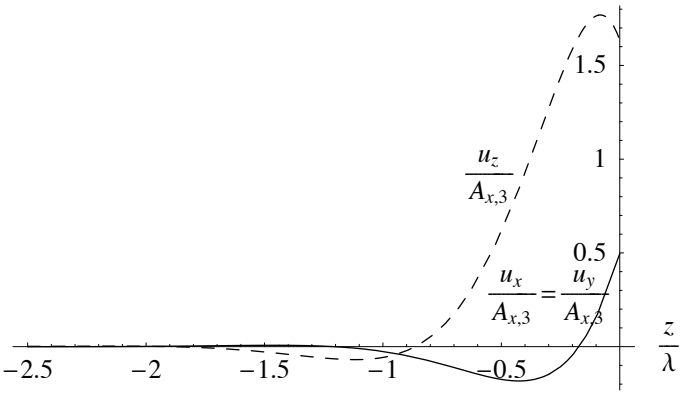


Figure 2.5: The variation of the two transverse components of the Rayleigh wave propagating in the [110] direction, as a function of depth (in wavelengths).

## 2.2.2 Allowed Velocities

The anisotropic nature of $Al_{0.3}\,Ga_{0.7}\,As$ leads to a dependence of the phase velocity on the direction of propagation. The condition of a vanishing boundary condition matrix determinant was satisfied for $\theta$ ranging between 0 and 45 ° in one degree steps, which occurred at the allowed velocities in those directions. The following figure, Fig. 2.6, shows these allowed velocities, as well a set of bulk and and so called pseudo-surface or 'leaky' wave velocities, as a function of propagation direction. These pseudo-surface modes are characterised by a decay in the direction of propagation as well as the radiating of energy away from the surface, and will be discussed in section 2.2.4.

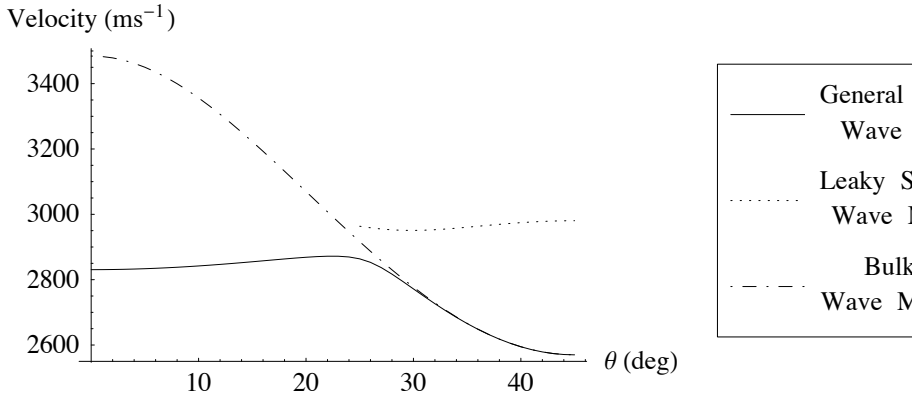


Figure 2.6: Surface, bulk and leaky wave velocities of as a function of propagation direction.

As seen in the figure at a value of around $\theta \sim 30\,°$, the SAW merges into a bulk wave - a transverse mode polarised in the sagittal plane, although surface wave solutions still exist along this branch up until $\theta = 45\,°$. Notice that at around $\theta \sim 25\,°$ a new kind of vibration appears associated to a pseudo-surface wave, which will be discussed in more detail later. These pseudo-surface waves, also known as 'leaky' surface waves, are characterised by a decay in the propagation direction as well as into the bulk. As the direction of propagation reaches 45° - the [110] direction, the leaky surface mode becomes a real surface wave, with a phase velocity of 2980.4 ms$^{-1}$.

A number[38–40] of theoretical studies of SAW propagation in these high symmetry directions for $Al_x\,Ga_{1-x}\,As$ have been made - although any theoretical treatment of SAW propagation in the (001) plane of cubic crystals, for which there are many,[5,7,11,33] with the elastic constants of

$Al_x\,Ga_{1-x}\,As$ used could be used for comparison. Adachi[40] gives explicit formulae for the velocities in terms of the elastic constants:

$$c_{11}\left(V^2 - \frac{c_{44}}{\rho}\right)\left(V^2 - \frac{c_{11}}{\rho} + \frac{{c_{12}}^2}{c_{11}\,\rho}\right)^2 = c_{44}\,V^4\left(V^2 - \frac{c_{11}}{\rho}\right)$$

$$c_{11}\left(V^2 - \frac{c_{44}}{\rho}\right)\left(V^2 - \frac{2\,c_{44} + c_{12} + c_{11}}{2\,\rho} + \frac{{c_{12}}^2}{c_{11}\,\rho}\right)^2 ==$$

$$c_{44}\,V^4\left(V^2 - \frac{2\,c_{44} + c_{12} + c_{11}}{2\,\rho}\right)$$

for the [100] and [110] propagation direction, respectively. Using the same elastic constants, these equations yield the precise velocities (to 7 significant figures) as those calculated here.

Another interesting representation of the calculated SAW velocities is shown in Fig. 2.7 - a polar plot for all angles from 0 to $2\pi$, for the general surface wave branch depicted in the previous figure.

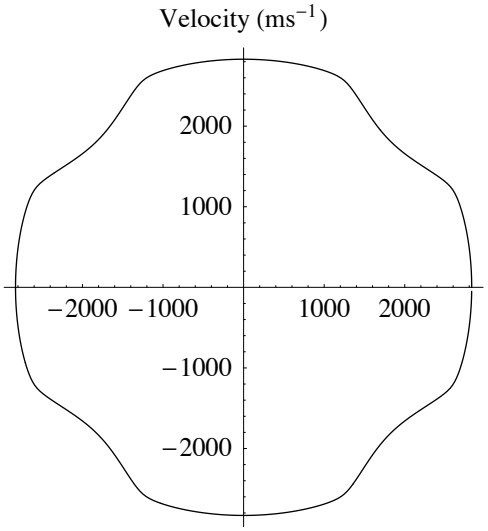


Figure 2.7: Polar plot of the surface wave velocities for all propagation directions on the (001) plane.

There is limited experimental data for surface wave velocities on $Al_x\,Ga_{1-x}\,As$. Sapriel[36] made measurements using Brillouin scattering techniques, for a range of doping densities $x$ in the high symmetry directions, [100] and [110]. Whilst no measurements were made for $x = 0.3$, a highly correlated linear relationship between measured velocities and concentration $x$ was produced, giving velocities of 2777 ms$^{-1}$ and 2911.5 ms$^{-1}$ for the [100] and [110] directions respec-

tively. This corresponds to a 1.8% and 2.3% difference in the calculated results above of $2830.6\,\mathrm{ms}^{-1}$ and $2980.4\,\mathrm{ms}^{-1}$. Although these results do not include piezoelectric effects, it is shown later in chapter three that there is only very small variation in SAW velocities, at most 0.1%, when piezoelectricity is considered. A more recent study[37] using a standard split-finger interdigitated transducer yielded a velocity in the [110] direction as $2968.5\,\mathrm{ms}^{-1}$, corresponding to an error of only 0.4%.

Discrepancies between these measured and calculated velocities may be attributed to a number of factors. Although the assumption of a linear relationship between concentration $x$ and the elastic constants, which was used here, is widely accepted,[37–41] their is some argument[36] that the elastic constants may undergo a "*softening*" for increasing values of $x$ in the $\mathrm{Al}_x\,\mathrm{Ga}_{1-x}\,\mathrm{As}$ alloy, where for higher values of $x$ a linear approximation is not valid.

### 2.2.3 Decay Constants

The very definition of surface waves, whether they be electromagnetic, elastic, or otherwise, describe a mode of propagation of energy along a free surface whereby the amplitude of the wave undergoes exponential decay below this surface. Therefore it is common to talk of a constant which quantifies this decay, namely the decay constant.

The method of solving for the surface modes outlined at the start of the chapter yields three decay constants $\kappa_1$, $\kappa_2$ and $\kappa_3$, the three lower-half complex plane roots of the secular equation (Eqn. 2.6). Each represent the z-component of the wavevector of each of the plane wave solutions contributing to final surface wave solution, a superposition of these three waves.

Solving the surface wave problem for an isotropic media leads to purely imaginary decay constants - and thus purely exponential decay into the bulk of the material. In the case of anisotropic media, some if not all of the decay constants attain both a real and imaginary component. The consequence of this are surface waves that exhibit sinusoidal decay into the bulk, and are known as Rayleigh waves.

As mentioned previously, these decay constants depend upon the allowed velocity of the SAW - which acts as parameter in the explicit form of each $\kappa_r$, and is determined from the condition of a vanishing boundary condition determinant. Plots of each $\kappa_r$ as a function of velocity for the case $\theta = \frac{\pi}{3}$ can be seen in Fig. 2.8.

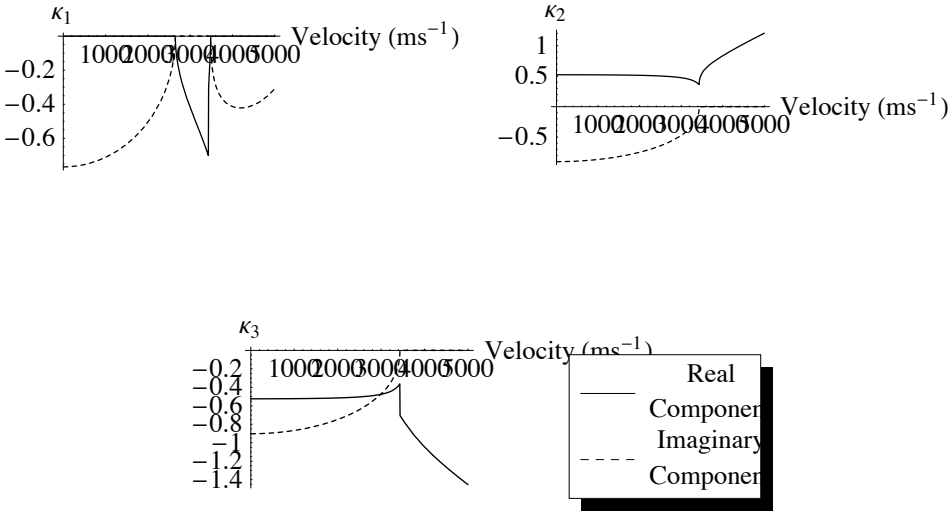


Figure 2.8: The three decay constants, $\kappa_1$, $\kappa_2$ and $\kappa_3$ as a function of velocity for $\theta = \frac{\pi}{3}$.

Consider the plot of $\kappa_1$. Notice that for $0 \geq V > 2780\ \text{ms}^{-1}$ the decay constant remains purely imaginary, and thus the first component of the superposition will not involve an oscillatory decay into the bulk, but rather just a purely exponential one - much alike to the decay expected in the isotropic case. It then changes from purely imaginary to purely real over the range $2780 > V > 3484\ \text{ms}^{-1}$. If the allowed velocity happened to be within this range, the corresponding component of the solution would not decay away from the surface, and would not be considered a surface wave - but rather a bulk wave. The plots of $\kappa_2$ and $\kappa_3$ show the complex form which typify Rayleigh wave solutions. The real components are identical but with opposite signs for $\kappa_2$ and $\kappa_3$ - and are responsible for the oscillatory nature of the decay. There exists a cut-off velocity at which there ceases to be surface wave solutions - that is, the decay constant ceases to have a negative imaginary component. It happens to correspond to the velocity of one of the bulk transverse waves, which remains invariant regardless of the propagation direction:

$$V_{\text{cutoff}} = \sqrt{\frac{c_{44}}{\rho}} = 3484.5\ \text{ms}^{-1}$$

For all directions of propagation over the (001) plane of $Al_{0.3}\ Ga_{0.7}\ As$, the allowed velocities are less than this bulk transverse wave velocity, and thus correspond to surface wave solutions.

The three plots of Fig. 2.9 show the values of the decay constant for a range of propagation directions.

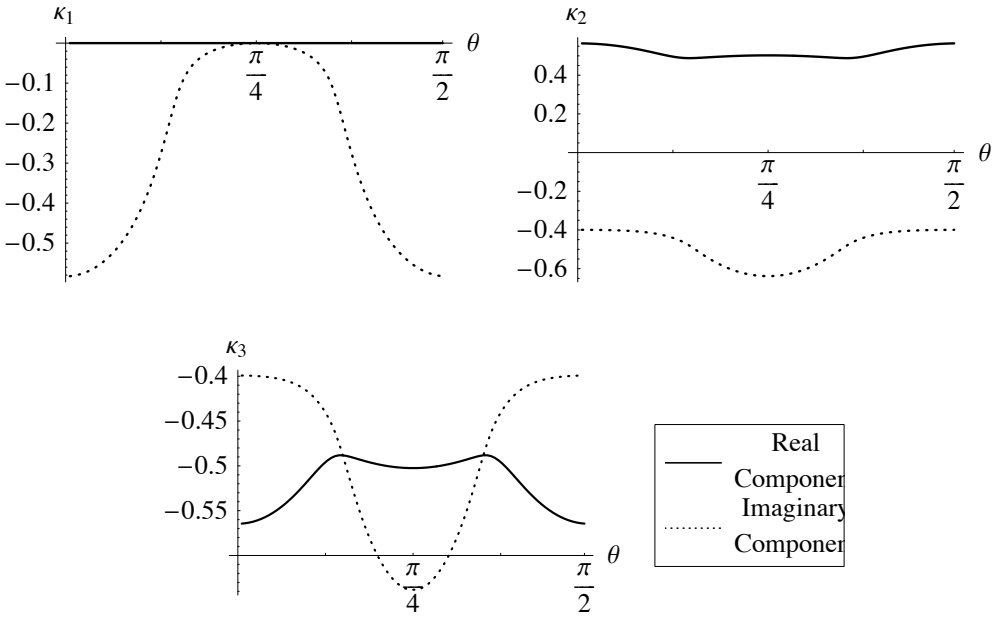


Figure 2.9: Values for each decay constant for different directions of propagation

For $\kappa_2$ and $\kappa_3$, a variation of no more than 0.25 in the real and imaginary components occurs over the range of propagation directions. For these two decay constants, fastest decay of their corresponding plane wave components will occur at $\theta = \frac{\pi}{4}$, where the magnitude of the imaginary component is the largest, and slowest decay at $\theta = 0, \frac{\pi}{2}$. The first decay constant, $\kappa_1$ shows some interesting behaviour as the propagation direction approaches $\theta = 45°$. The real component is zero for all propagation directions, and as $\theta$ approaches 45° it moves closer and closer to the origin of the complex plane, giving ever deeper penetration to the displacement. In the [110] direction (ie $\theta = 45°$), $\kappa_1 = 0$, and the solution has degenerated completely into the bulk wave.

A possible quantification of the decay into the bulk can be made by using an analogy to the 'skin-depth', $\delta$, of electromagnetic theory, a depth at which the amplitude of the EM wave travelling in a dielectric media decays to $\frac{1}{e}$ of its original value. The complex nature of the amplitudes and decay constants makes it difficult to establish a value for each skin depth for the superposition solution - and only approximate results can be produced based upon numerical solutions. Instead, the imaginary parts of each of the decay constants are considered separately, where

$$\delta_r = -\frac{1}{2\pi\,\mathrm{Im}(\kappa_r)}$$

This gives a very basic representation of the decay length for each component, which is seen in Fig. 2.10

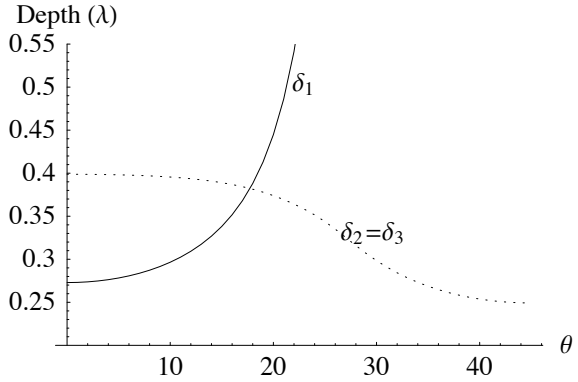


Figure 2.10: The relative variation of decay depth (in wavelengths) for each component of the surface wave solution for different propagation directions.

Although this doesn't give an entirely correct representation of the decay length of the complete surface wave solution, it does provide some information on the relative effect of each decay constant as the propagation direction changes. As the propagation direction tends toward 45°, $\kappa_1$ decreases to zero the corresponding decay length, $\delta_1$, diverges to infinity - whilst $\delta_2$ and $\delta_3$, which are equal, remain finite - varying by only 0.15 wavelengths over this range.

A better representation of the effect of each of the decay constants can be provided by weighting coefficients that represent the contribution from each term in the SAW solution, which can be defined as

$$\alpha_r = (A_{x,r} + A_{y,r} + A_{z,r})$$

These weighting coefficients, suitably normalised, are depicted in Fig. 2.11 They provide an explaination of the degeneration of the surface mode into a bulk mode as the propagation direction approaches [110], shown in Fig. 2.6. The weighting coefficient $\alpha_1$ that corresponds to the first decay constant $\kappa_1$ gives no contribution to the final solution at [100], which is verified later in the chapter. Both $\alpha_2$ and $\alpha_3$ give equal contributions to the solution for all directions of propagation; the largest for [100], and nothing at [110]. The contribution $\alpha_1$ becomes larger as $\theta$ increases, when at 45° the other contributions to the solution, $\alpha_2$ and $\alpha_3$, vanish completely. In this high symmetry direction the superposition breaks down entirely to a single component, now

only depending upon the first decay constant, $\kappa_1$. As was shown earlier, the imaginary part of $\kappa_1$ vanishes in the [110] direction - and thus the solution ceases to satisfy the condition for surface waves - that it exhibits exponential decays away from the free surface into the bulk. The solution has become a transverse bulk wave, polarised in the plane perpendicular to the sagittal plane, with phase velocity of 2569.9 $ms^{-1}$ - lower than all surface wave solutions on the (001) plane of $Al_{0.3}$ $Ga_{0.7}$ As.

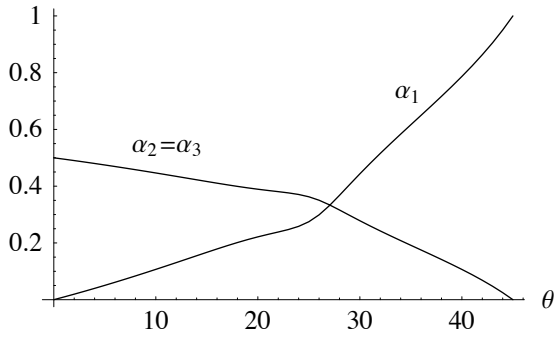


Figure 2.11: Weighting coefficients associated with each term of the final SAW solution, as a function of propagation direction.

### 2.2.4 Leaky Surface Waves

The surface wave solution found the [110] direction is quite unique in the fact that it is quite isolated from other surface wave solutions on the (001) plane and it is the only surface wave on this plane with a phase velocity higher than the lowest bulk wave velocity. This only occurs in a very limited set of directions for particular anisotropic surfaces. The branch of velocities depicted in Fig. 2.6 do not correspond to real surface acoustic waves - but rather solutions known as 'pseudo-surface' or 'leaky' waves. These velocities only correspond to very approximate zeros of the determinant - while the real component was zero for this velocity, the imaginary component remains very small but non zero - on the order of $10^{-3} - 10^{-6}$. A good example is the plot of the boundary condition matrix for $\theta = 30°$, Fig. 2.3. As a consequence they will not exactly satisfy the stress free boundary conditions. Fig. 2.12 gives a table of the absolute values of the determinant evaluated at the approximate velocities of the leaky surface waves.

| | | | | | | | |
|---|---|---|---|---|---|---|---|
| 25° | $3.6\times10^{-3}$ | 30° | $2.7\times10^{-4}$ | 35° | $7.2\times10^{-5}$ | 40° | $1.4\times10^{-4}$ |
| 26° | $2.5\times10^{-3}$ | 31° | $9.8\times10^{-6}$ | 36° | $1.2\times10^{-4}$ | 41° | $1.0\times10^{-4}$ |
| 27° | $1.7\times10^{-3}$ | 32° | $1.6\times10^{-5}$ | 37° | $1.5\times10^{-4}$ | 42° | $6.7\times10^{-5}$ |
| 28° | $1.0\times10^{-3}$ | 33° | $1.1\times10^{-6}$ | 38° | $1.7\times10^{-4}$ | 43° | $3.3\times10^{-6}$ |
| 29° | $5.8\times10^{-4}$ | 34° | $2.7\times10^{-5}$ | 39° | $1.6\times10^{-4}$ | 44° | $8.6\times10^{-6}$ |

Figure 2.12: Absolute values of the boundary condition determinant evaluated at the approximate allowed velocities of the leaky waves, which appear between in propagation directions 25° and 44°.

If the components of the wave vector $k_{||}$ are allowed to have small imaginary components, corresponding to an attenuation in the direction of propagation, then the associated allowed velocities would give solutions that would completely satisfy the stress free boundary conditions. For the isolated direction itself, the Rayleigh type solution has two associated complex decay constants, whereas for angles near this direction the solutions involve a small third term representing a quasi-transverse bulk wave with its propagation vector in the sagittal plane but tilted down into the solid. Therefore this wave does not satisfy the condition that the displacement components vanish at an infinite depth below the surface. Although the imaginary component is quite small for angles close to the isolate direction - and so decay is quite slow, and thus experimental conditions for surfaces waves are easily observeable. As the propagation vector deviates further from this direction coupling between the bulk mode becomes much stronger, and the amount of energy radiated away from the surface increases dramatically. So, although the obey the stress free boundary conditions, they are strictly not surface waves and the term 'leaky' surface waves, borrowed from electromagnetic theory, is appropriate - reflected the slow leak of energy into the bulk. Special consideration must be given to these solutions when considering surface wave propagation in the [110] direction of the (001) plane of cubic crystals.

### 2.2.5 Amplitude Profiles

Another important aspect of the surface wave is the actual amplitudes of displacement, and the associated polarisation of such displacements as the direction of propagation changes. Figure 2.13 shows these relative amplitudes as measured along the cartesian axes, for a variety of different depths beneath the surface.

In terms of acoustic charge transport phenomena, it is important to understand the nature of the these elastic polarisations, which in turn produce the piezoelectric fields. These fields and the associated potential are discussed in chapter three.

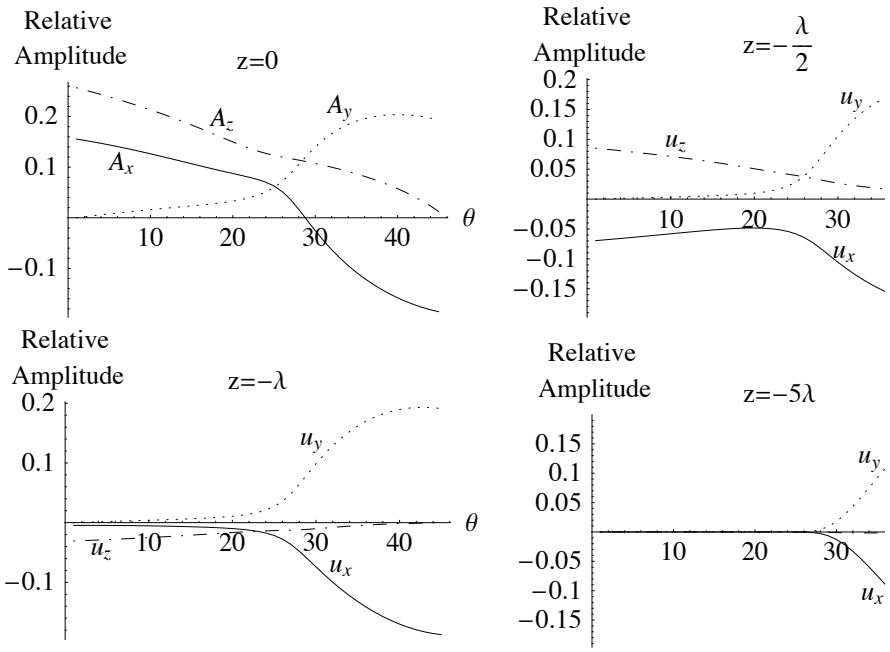


Figure 2.13: Relative displacement amplitudes as measured along the cartesian axes, as a function of propagation direction for different depths beneath the surface.

Notice at all depths in the x-direction, the y-component of displacement is absent - and displacements are confined to the sagittal plane with a transverse z-component and longitudinal x-component, as was shown previously. The purely transverse mode of propagation can be seen in the y-direction, at 45°; where $u_x = -u_y$. The in this case, z-component is absent and displacements are confined parallel to the surface. Surface modes degenerate into this bulk mode as the direction of propagation $\theta$ increases - notice at a depth of 5 wavelengths where all displacements between 0° and ~27° have vanished, this mode, which satisfies the stress free boundary conditions shows no signs of attenuation. The oscillatory decay associated with Raleigh solutions can also be seen in Fig. 2.13 – notice that for different depths the sign of particular amplitude components change.

Fig. 2.14 shows the amplitudes as contributions to the surface displacement in terms of two transverse and one longitudinal component for the general surface wave branch, and that part of the leaky wave branch nearby [110]. The longitudinal component, $U_L$, is surface displacement measured along the wavevector $\boldsymbol{k}_{||}$, the vertical transverse component, $U_V$, corresponds to the displacement perpendicular to the surface, and the other transverse component, $U_T$, is measured perpendicular to the sagittal plane, or a vector defined as $\boldsymbol{k}_{\perp}$. In terms of the cartesian amplitudes $A_x$, $A_y$ and $A_z$, these are expressed as

$$U_L = \frac{k_{\|} \cdot (A_x, A_y)}{|k_{\|}|} \qquad U_V = A_z \qquad U_T = \frac{k_{\perp} \cdot (A_x, A_y)}{|k_{\perp}|}$$

As the weighting coefficients indicated that the contributions of the second and third terms in the final surface wave solution were equivalent, the sum of these components are presented in Fig. 2.14 along with the first term contribution of each of the surface displacements.

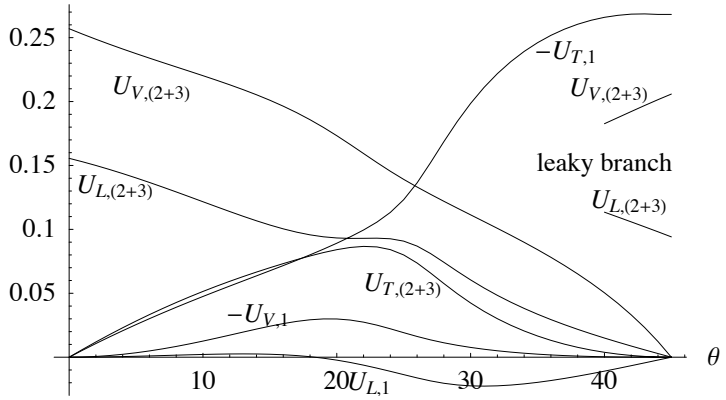


Normalised surface displacement components corresponding to each $\kappa_r$:
Figure 2.14: $U_{T,r}$: Transverse components parallel to the sagittal plane; $U_{V,r}$: Transverse components perpendicular to the surface; and $U_{L,r}$: Longitudinal component parallel to $k_{\|}$

As expected, the only contribution to the surface displacement at 45° is the first term of the transverse component - the bulk mode. Likewise for 0°, where only vertical and longitudinal displacements exist. The longitudinal and vertical components dominate the solution up until the surface wave begins to degenerate into the bulk wave. The polarisation of the leaky surface wave involves a vertical and longitudinal component - and a small transverse component, which is not shown on the figure.

# Chapter Three: Piezoelectric Surface Acoustic Waves

The piezoelectric effects of $Al_{0.3}\,Ga_{0.7}As$ are sufficiently small such that it could be neglected in the formulation of the surface wave problem. Although, as interest lies in the associated potential that accompanies the surface waves on this piezoelectric material, such effects are included.

The method of finding surface wave solutions for the piezoelectric case is very similar to that used for non-piezoelectric elastic waves, which was outlined in chapter two. The addition of piezoelectricity complicates further the solution of surface waves by increasing to four the number of partial waves, by introducing terms containing the potential into the zero-stress boundary condition, and by requiring consideration of the electric boundary conditions at the surface.

This chapter discusses these SAW solutions, and how they compare to the non – piezoelectric surface wave results. Discussion of the piezoelectric fields and potential associated with the SAW is also included, with an emphasis on how they vary with direction and distance below the surface. As will be seen in chapter four, the importance of the direction of propagation and depth of the 2DEG is paramount when considering acoustic charge transport phenomena.

## 3.1 Theory and Method

The method used to solve for piezoelectric surface acoustic waves is very similar to the method used in chapter two. A complete discussion can be found in appendix A4, and only a summary is presented here.

The wave equations that govern piezoelectric surface acoustic waves are

$$\rho \frac{\partial^2 u_x}{\partial t^2} = c_{11} \frac{\partial^2 u_x}{\partial x^2} + c_{44}\left(\frac{\partial^2 u_x}{\partial y^2} + \frac{\partial^2 u_x}{\partial z^2}\right) + (c_{12} + c_{44})\left(\frac{\partial^2 u_y}{\partial x\,\partial y} + \frac{\partial^2 u_z}{\partial x\,\partial z}\right) + 2\,e_{14}\frac{\partial^2 \phi}{\partial y\,\partial z}$$

$$\rho \frac{\partial^2 u_y}{\partial t^2} = c_{11} \frac{\partial^2 u_y}{\partial y^2} + c_{44}\left(\frac{\partial^2 u_y}{\partial x^2} + \frac{\partial^2 u_y}{\partial z^2}\right) + (c_{12} + c_{44})\left(\frac{\partial^2 u_x}{\partial x\,\partial y} + \frac{\partial^2 u_z}{\partial y\,\partial z}\right) + 2\,e_{14}\frac{\partial^2 \phi}{\partial x\,\partial z}$$

$$\rho \frac{\partial^2 u_z}{\partial t^2} = c_{11} \frac{\partial^2 u_z}{\partial z^2} + c_{44} \left( \frac{\partial^2 u_z}{\partial x^2} + \frac{\partial^2 u_z}{\partial y^2} \right) +$$

$$(c_{12} + c_{44}) \left( \frac{\partial^2 u_x}{\partial x \partial z} + \frac{\partial^2 u_y}{\partial y \partial z} \right) + 2 e_{14} \frac{\partial^2 \phi}{\partial x \partial y}$$

$$2 e_{14} \frac{\partial^2 u_x}{\partial y \partial z} + 2 e_{14} \frac{\partial^2 u_y}{\partial x \partial z} + 2 e_{14} \frac{\partial^2 u_z}{\partial x \partial y} = \epsilon \nabla^2 \phi$$

These equations are formulated into a 4×4 matrix, and the condition of a vanishing determinant is used to find the four decay constants. As a result, surface wave solutions are the superposition of four plane wave solutions, each satisfying the boundary conditions associated with a piezoelectric surface.

In addition to the stress-free boundary conditions, piezoelectricity introduces an electric boundary condition. This requires the continuity of the normal component of the electric displacement over the surface, which is expressed as:

$$e_{14} \left( \frac{\partial u_x}{\partial y} + \frac{\partial u_y}{\partial x} \right) - \epsilon \frac{\partial \phi}{\partial z} - \epsilon_o k_{||} \phi = 0 \qquad at \quad z = 0$$

This boundary condition, in addition to the three stress free equations are combined into a 4×4 boundary condition matrix. The velocities that see the determinant of this matrix vanish correspond to the allowed velocities of the piezoelectric SAW.

## 3.2 Results and Discussion

The alloy $Al_x Ga_{1-x} As$ is weakly piezoelectric. Its electromechanical coupling constant is one-sixteenth of $LiNbO_3$, and half of that for quartz. As a result, the introduction of piezoelectric terms in the wave equation and boundary conditions have a very little effect on the elastic properties of surface acoustic waves. Despite the relative low coupling, the piezoelectric fields and potential associated with these elastic waves are significant. It is this reason that acoustic charge transport occurs, so a thorough understanding of these quantities is important.

Previous research for SAW propagation in arbitrary directions for piezoelectric crystals[35,45] concentrate on features for certain elastic experiments and device applications. Literature searches failed to recover any publications regarding features important for acoustic charge transport, particularly in AlGaAs. This new research is based on calculations made for the same orientation and range of propagation directions in chapter two, and includes:

-analysis of the four decay constants to explain SAW properties;
-the variation of the piezoelectric fields for different depths; and
-profiles of the electric potential

### 3.2.1 High symmetry directions

*Propagation in the [100] direction*

Surface acoustic wave propagation on the (001) plane of piezoelectric cubic crystals has been extensively studied in the high symmetry directions[11,12,33]. For propagation along the [100] direction, the wave equation matrix defined in Eqn. 0.36 becomes:

$$\mathcal{M} = \begin{pmatrix} c_{44}\,k^2 - V^2\,\rho + c_{11} & 0 & k\,(c_{12} + c_{44}) & 0 \\ 0 & (k^2+1)\,c_{44} - V^2\,\rho & 0 & 2\,k\,e_{14} \\ k\,(c_{12} + c_{44}) & 0 & c_{11}\,k^2 - V^2\,\rho + c_{44} & 0 \\ 0 & 2\,k\,e_{14} & 0 & (-k^2-1)\,\epsilon \end{pmatrix}$$

Notice now there are two possible modes. One is a non-piezoelectric two component Raleigh wave with components polarised in the sagittal plane:

$$\begin{pmatrix} c_{44}\,k^2 - V^2\,\rho + c_{11} & k\,(c_{12} + c_{44}) \\ k\,(c_{12} + c_{44}) & c_{11}\,k^2 - V^2\,\rho + c_{44} \end{pmatrix} \begin{pmatrix} A_x \\ A_z \end{pmatrix} = 0$$

And the other a single component piezoelectric surface wave polarised orthogonal to the sagittal plane, coupled to an electric field.

$$\begin{pmatrix} (k^2+1)\,c_{44} - V^2\,\rho & 2\,k\,e_{14} \\ 2\,k\,e_{14} & (-k^2-1)\,\epsilon \end{pmatrix} \begin{pmatrix} A_y \\ A_\phi \end{pmatrix} = 0$$

The associated boundary conditions also separate accordingly. The two component Raleigh wave is simply the SAW solved for the non-piezoelectric case in the [100] direction, Fig. 2.4 The second set of equations correspond to a surface wave solution known as a Bleustein-Gulyaev wave. Although for this plane of propagation, no zeros of the associated boundary condition matrix were found - so no solution exists in this direction. Bleustein-Gulyaev waves are found only to exist[35] along the $[1\bar{1}0]$ direction in the (110) plane of cubic crystals.

From a crystallographic point of view, the surface wave propagating in the [100] direction induces strains in the [100] (longitudinal) and [001] (transverse) directions. Neither of these are polar directions in the zinc-blende structure, and thus do set up polarisations with the crystal.

*Propagation in the [110] direction*

Many experiments investigating acoustic charge transport involve SAW propagation in the [110] direction of the (001) plane piezoelectric cubic crystals, or equivalent directions. In section 4.2.3 this direction is studied in greater detail, and it is shown that surface wave propagation in this direction has the highest associated electromechanical coupling and largest piezoelectric potential.

Solving the piezoelectric wave equation in this direction yields a solution whose displacements are polarised in the sagittal plane - a longitudinal component and a transverse vertical component. This is known as a two component Raleigh wave, and is identical to the solution found in chapter two – except with a phase velocity of 2983.6 $ms^{-1}$, 0.11% higher than the uncoupled case.

### 3.2.2 Allowed Velocities and Decay Constants

As a result of such weak coupling, the surface wave velocities differ only slightly when piezoelectric effects are included. Fig. 3.1 shows the difference between the calculated velocities. For the surface wave branch, the largest difference in velocities occurs at around $\theta \sim 24°$, just below 2 $ms^{-1}$, which corresponds to a 0.06% change. This is an argument that this direction of propagation has associated with it the highest electromechanical coupling for the branch of surface waves that degenerate into bulk modes, which is verified in section 3.2.3. The velocities for the leaky surface modes were also calculated, and were found to differ from the non piezoelectric leaky waves by no more than 0.1%. Although the coupling was not investigated for the leaky modes, the difference in velocity reflects a relatively high coupling strength.

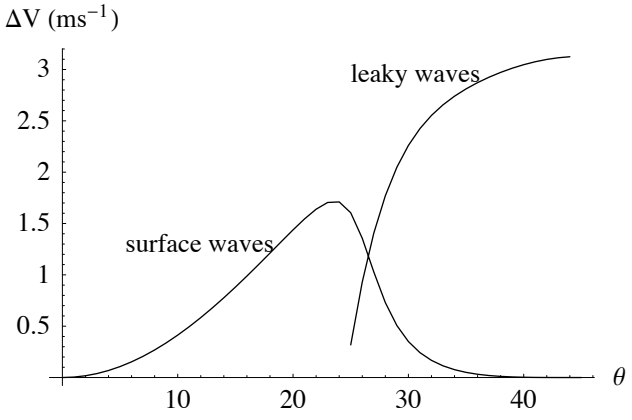


Figure 3.1: The difference in calculated SAW velocities when piezoelectric coupling is considered.

As mentioned in section A.4.4, the introduction of an additional term in the wave equation leads to an eighth order secular equation, and thus four decay constants. Three of these four roots are essential the same to the roots defined in chapter three. The additional decay constant, defined as the first, $\kappa_1$, is purely imaginary over all propagation directions. It is the least varying of all the roots, as can be seen in Fig. 3.2. The nature of this root is much alike those found for isotropic substrates - purely imaginary and constant over all directions, which reflects the strength of the piezoelectric coupling. As the magnitude of piezoelectric constant $e_{14}$ is increased, the variation in $\kappa_1$ increases. Another interesting aspect of this root is its relative magnitude. Consider the values of the decay constants for $\theta = 15\,°$: $\kappa_1 = -1.015\,i$, $\kappa_2 = -0.463\,i$, and $\kappa_{3,4} = \pm 0.532 - 0.408\,i$. The new root has the largest imaginary component, and for propagation in this direction, a corresponding 'skin depth' of 0.16 wavelengths. This contribution to the solution is highly localised at the surface and exhibits the fastest rate of decay into the bulk, and as it turns out - is the smallest contributing term in the solution. At the surface this term contributes at most 2% of the total displacement, further confirming the very weak effect piezocoupling effects of $Al_{0.3}\,Ga_{0.7}\,As$.

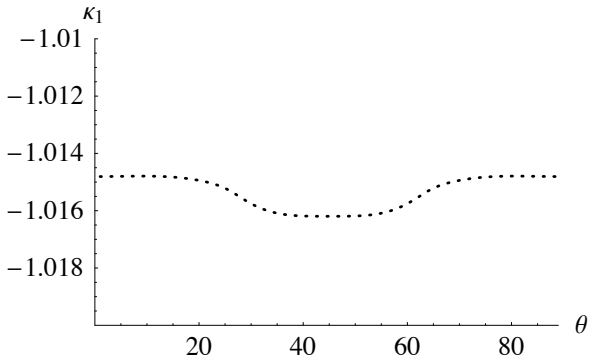


Figure 3.2: The purely imaginary additional decay constant associated with the piezoelectric SAW solutions, for different directions of propagation.

### 3.2.3 Piezoelectric fields and potential

*Electromechanical coupling*

Traditionally the strength of piezoelectric coupling is quantified by the electromechanical coupling constant, K. For bulk waves, $\frac{K^2}{2}$ is an explicitly calculable factor containing the terms $\frac{e_{ijk}{}^2}{c_{ijkl}\,\epsilon_{ij}}$, which also defines the fractional increase in the velocity produced by piezoelectricity. However, for surface waves, because of their inhomogeneity in the direction normal to the surface, there is no corresponding explicit electromechanical coupling factor. It is nevertheless important to have a single parameter to express this coupling: one that is useful for device analysis and is easily measurable and calculable. In analogy with the bulk wave case, an effective electromechanical coupling factor is defined as twice the fractional change in surface wave velocity produced by electrically shorting the mechanically free surface of the piezoelectric substrate[35]:

$$\frac{K^2}{2} = \frac{V - V_s}{V} \tag{3.1}$$

where $V$ is the surface wave velocity with the free surface and $V_s$ with it shorted. Calculation of SAW velocities with an electrically shorted surface requires a manipulation of the electrical boundary conditions such that the sum of the terms in the potential is zero at the surface. In terms of the boundary condition matrix (Eqn. 3.20), the fourth row is replaced by $b_{4r} = 1$. Fig. 3.3 shows the relative variation in the electromechanical coupling constant as a function of direction.

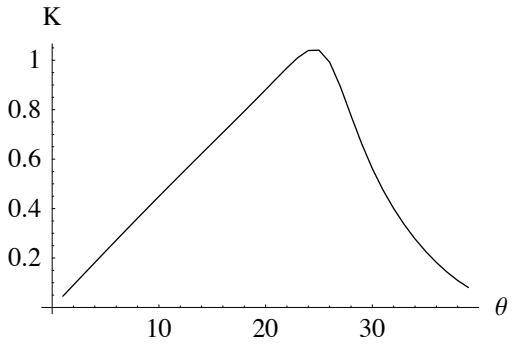


Figure 3.3: Normalised values of the electromechanical coupling constant for the surface wave branch, as a function of direction.

Notice that the highest value of K for the surface wave branch occurs at $\theta \sim 25°$. Unfortunately, due to the gradual degeneration of the SAW into a transverse bulk mode for directions past

$\theta \sim 30°$, values for K shown in Fig. 3.3 do not reflect the strength of the coupling for larger angles. In effect, the transverse bulk elastic displacements that dominate at these angles are perpendicular to the polar direction [111], and there is no corresponding piezoelectric field.

### *Variation of Electric potential*

Two main aspects of the potential associated with a propagating SAW has been investigated - how it varies with propagation direction, and with depth. There are four amplitudes contributing to the potential, each corresponding to one of the four decay constants. It is these terms, defined in Eqn. 0.38, that governs the electric potential's behaviour. All potentials have been normalised to the value at a depth of 0.1 wavelengths for $\theta = 33°$.

The piezoelectric potential shows some very interesting behaviour over the range of propagation directions. Fig. 3.4 shows the total potential for five different depths, as a function of direction. As discussed previously, the [100] direction exhibits no piezoelectric properties and the potential at all depths is zero. As the angle from [100] is increased, the elastic displacements (as discussed in section 2.2.5) induce strain components in the polar direction [111]. The corresponding potential that results from the induced electric fields is approximately the same for all depths, although when the angle reaches around 21°, these potentials diverge suddenly from one another. Those closer to the surface increase up to twice their value over the span of only 10°, whilst depths below a quarter of a wavelength decrease in value. The potential close to the surface peaks in the propagation direction ~33° from the x-axis, and drops to zero as quickly as it increased. The potential is zero for the bulk wave solution at [110], for all depths - as expected based on arguments discussed in the previous section..

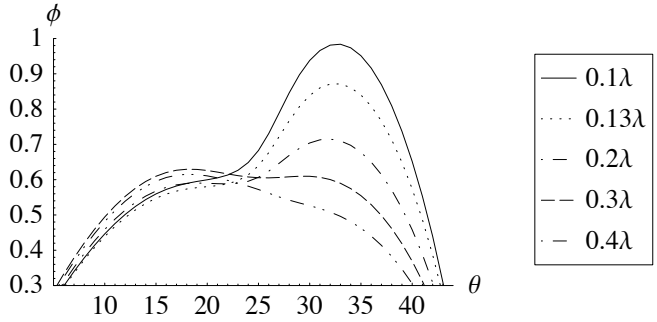


Figure 3.4: Normalised piezoelectric potential as a function of direction for different depths.

To understand the unusual variation of this potential over different directions it is important to consider each of the components that contributes to the total potential. The four terms, each corresponding to one of the four decay constants, are depicted as a function of propagation

direction in Fig. 3.5 for three different depths. The most significant contribution comes from the first term, which corresponds to the additional decay constant $\kappa_1$ that was included in the SAW solutions. This term contributes the least to the elastic displacements. The second term, whose associated decay constant is identified with the bulk mode, is effectively zero for angles $\theta \gtrsim 40\,°$, further indicating the zero coupling associated the bulk mode. The variation in the third and fourth components reflect the complex decay constants $\kappa_3$ and $\kappa_4$. As the depth increases, the third component gives a greater relative contribution to the final potential. Akin to the elastic displacements, oscillatory decay of the potential also occurs, which is an explanation for the significant variation over the range of different depths.

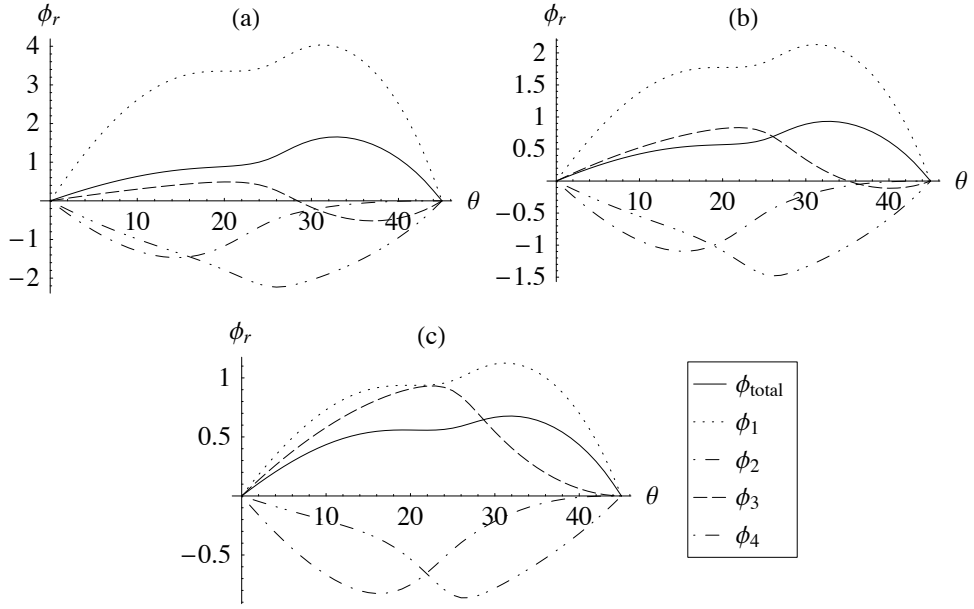


Figure 3.5: The relative values of the each component contributing to the potential, as a function of direction, for three different depths: (a) $z = 0$, (b) $z = 0.1\,\lambda$; and (c) $z = 0.2\,\lambda$

The variation as a function of depth is shown in Fig. 3.6, for four different directions. The most striking characteristic of these plots is the form at small depths for $\theta = 10\,°$ and 20°, which is a direct consequence of the complex decay constants. A local minima is evident at around 0.15 wavelengths below the surface - and this potential well structure has a significant physical consequence in acoustic charge transport, which will be discussed in section 4.2. As the direction of propagation goes from $20\,° \rightarrow 30\,°$, the contribution near the surface of the third and fourth terms begins to diminish, this minima vanishes, and the decay of the potential attains a common exponential form. The plot for $\theta = 30\,°$ demonstrates the slow decay associated with the second

term. As mentioned previously, its amplitude decreases and the decay length increases as it approaches the [110] direction − evident in the fourth plot, $\theta = 45°$. Here the decay is almost purely exponential - due to the heavy weighting of the first term which has a imaginary decay constant, although for $z >> \lambda$ the potential is very small but remains non-zero.

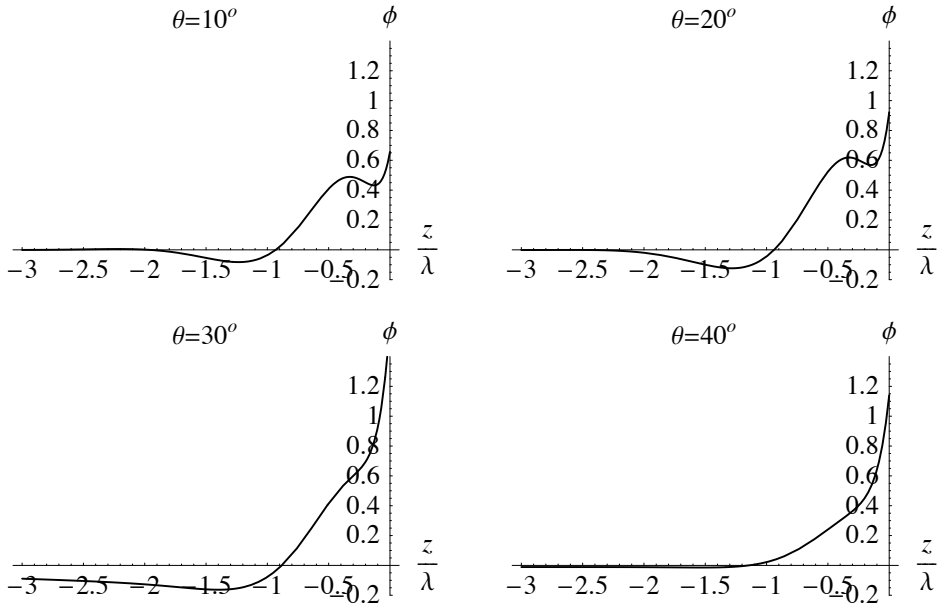


Figure 3.6: Plots of the potential as a function of depth.

## *Piezoelectric fields*

The piezoelectric fields associated with the travelling SAW can be directly calculated from the potential:

$$\boldsymbol{E} = -\nabla\phi$$

The electric potential has a wave-like dependence, and alike the elastic displacements, planes of constant phase are perpendicular to the sagittal plane. As a result, regardless of the propagation direction, there is no transverse component of electric field. The fields at a depth $z = z_o$ measured in the two frames of reference are:

$$E_x = -i\,k_{\|}\,\mathrm{Cos}(\theta)\,\phi(z_o) \qquad E_y = -i\,k_{\|}\,\mathrm{Sin}(\theta)\,\phi(z_o) \qquad E_z = -i\,k_{\|}\,\kappa_r\,\phi(z_o)$$

$$E_L = \frac{k_{\|}\cdot(E_x, E_y)}{|\,k_{\|}\,|} = \tag{3.2}$$

$$-i\,k_{\|}\,\phi(z_o) \quad E_T = \frac{k_{\perp}\cdot(E_x, E_y)}{|\,k_{\perp}\,|} = 0 \quad E_V = -i\,k_{\|}\,\kappa_r\,\phi(z_o)$$

Figure 3.7 shows the longitudinal and vertical components of the SAW, as a function of direction, for a number of different depths. The local potential minima in the potential profiles in the $z-$direction discussed previously manifests regions of zero vertical electric field, which is evident in Fig. 3.7(a). As the form of the potential changes (Fig 3.6), so does the corresponding vertical electric field, whose value is highly dependent upon the depth below the surface. The longitudinal component is better behaved and Eqns. 3.2 indicate it is quite similar to the form of the potential, shown in Fig. 3.4.

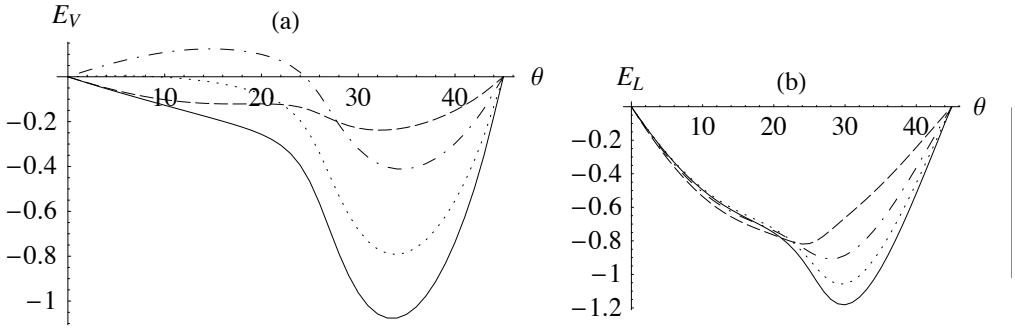


Figure 3.7: The relative Piezoelectric vertical (a) and longitudinal (b) fields as a function of propagation direction, for different depths (in wavelengths).

# Chapter Four: Acoustic Charge Transport

The following chapter includes an overview of the current theory of acoustic charge transport, as well as the discussion of a number of experiments conducted that give evidence for possible device applications. Now that all the characteristics of SAW propagation have been determined, it is important to consider some aspects relevant to acoustic charge transport. These include:

-phonon focusing effects on the (001) plane of AlGaAs;
-propagation directions best suited to ACT experiments;
-the location of the two-dimensional electron gas relative to the surface; and
-electron energy levels.

## 4.1 Phonon Focusing

Focusing phenomena of both bulk[46,47] and surface[48–50] phonons in anisotropic material has long been a topic of interest in condensed matter physics. This focusing of energy is not unique to the elastic regime - other elementary excitations, for example magnons or polaritons also have been shown[51] to display this effect. Focusing occurs in directions around selected pure modes of elastic propagation, which can be found by examining the angle between the Poynting vector and wavevector, or more graphically by considering a slowness surface.

### 4.1.1 Energy Flow

As for electromagnetic theory, energy transport in an elastic medium can be described by a Poynting vector. In the case of $Al_x Ga_{1-x} As$, whose piezoelectric coupling is very small, the associated electrical energy is negligible, so it can be neglected. In this case, the poynting vector components are defined as[33]:

$$P_i = -T_{ik} \frac{\partial u_i}{\partial t} = -i\omega T_{ik} u_i$$

The direction of the poynting vector describes the direction of energy transport, and its magnitude is equal to the amount of energy traversing a unit area per unit time. For pure surface wave modes there is no energy dissipation into the bulk and energy always travels parallel to the surface, and it is useful to define a power flow vector, which is

$$W_i = -\frac{1}{2} \int_{-\infty}^{0} P_i \, dz$$

where **W** represents the time averaged power crossing a strip of unit width and infinite depth oriented perpendicular to the vector. Analysis of the direction of power flow shows that only in a very few select directions it is colinear to the propagation vector. For computational purposes, the power flow, in terms of the surface wave displacements, is given by[35]

$$W_i = -\frac{1}{2}\,\mathrm{Re}\Big[\sum_{n=1}^{3}\sum_{m=1}^{3}\frac{\omega\, A_{k,n}\, A_{j,m}{}^{*}(c_{\mathrm{ijkl}} + c_{\mathrm{ijk3}}\,\kappa_n)}{i\,(\kappa_n - \kappa_m{}^{*})}\Big]$$

Surface waves do not radiate energy into the bulk, and $W_z = 0$, as expected. Examination of focusing effects can be made by comparing the angle between the propagation direction $\boldsymbol{k}_{\|}$ and the power flow vector **W**. Fig. 4.1 shows this angle, $\beta$, as a function of direction.

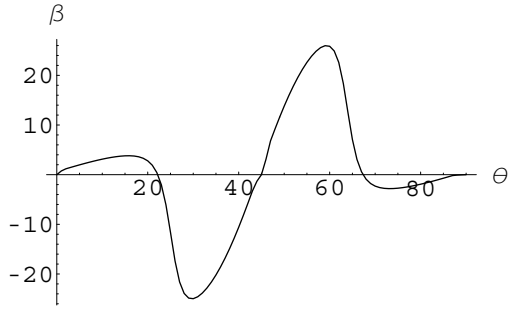


Figure 4.1: Angle (in degrees) between power flow vector **W** and $\boldsymbol{k}_{\|}$ for the range of propagation directions between [100] and [010].

As expected, the high symmetry directions, [100], [110] and [010] are all pure modes. Notice propagation & energy flow are also colinear at $\theta = 22.5\,°$ and $\theta = 67.5\,°$. At $\theta = 30\,°$, $60\,°$ the group velocity is at an angle of ~25° from the phase velocity - the largest deviation between energy flow and propagation direction.

### 4.1.2 Slowness surface

Slowness surfaces provide qualitive information on focusing effects. The slowness surface is a polar plot of constant frequency - the locus of the ends of the vectors $\boldsymbol{L} = \frac{\boldsymbol{k}_{\|}}{V}$. Since the group velocity is equal to the gradient of $\omega(\boldsymbol{k}_{\|})$, the direction of the group velocity in any direction is parallel to the normal to the slowness surface. Fig. 4.2 shows a slowness surface for the (001) plane of $Al_{0.3}\,Ga_{0.7}\,As$ between [100] and [010], for a SAW frequency of 1 GHz. Notice the pure modes at $\theta = 0\,°$, $22.5\,°$, $45\,°$, $67.5\,°$, $90\,°$ correspond to the zeros in Fig. 4.1, as expected.

Pure modes can be classified as concave or convex based upon the nature of adjacent points on the slowness surface, which characterises the two extremes of focusing. Concave pure modes

correspond to directions where energy flow it focused. As adjacent group velocities point inward toward the direction associated with the pure mode. The pure mode at 22.5° in Fig. 4.2 illustrates this. Convex pure modes on the other hand characterise where the energy flow of adjacent directions diverge, and the [110] direction in Fig. 4.2 is an example of this.

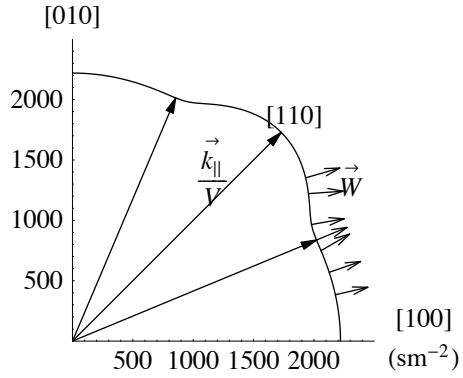


Figure 4.2: Slowness curve for the (001) plane of $Al_{0.3}$ $Ga_{0.7}$ As for $f$ = 1 GHz. Pure modes of propagation occur at 0°, 22.5°, 45°, 67.5° and 90°.

No slowness surface has been constructed for the leaky modes as energy is radiated into the bulk, and the above definition would be invalid. Instead if the energy propagation parallel to the sagittal plane was considered, the plot of velocities against direction (Fig. 2.6) indicates that there would be two pure modes. One in the [110] direction (the surface wave solution) and another at around $\theta \sim 30\,°$, although the slope of the plot implies that neither would exhibit focusing effects comparable to those of the surface wave branch.

# 4.2 Acoustic Charge Transport

## 4.2.1 Overview

When the piezoelectric potential accompanying a surface acoustic wave is coupled to a two – dimensional electron gas (2DEG) formed within a semiconductor heterostructure such as $Al_x\,Ga_{1-x}\,As/GaAs$, a phenomenon known as acoustic charge transport occurs. The interaction between the potential and the plasma results in an acoustoelectric current, of the order of nano-amps, during which the acoustic wave's amplitude and velocity both attenuate. The acoustoelectric drag effect, whereby the surface wave exerts a pressure on the electron gas was long thought a valid explanation[25] for this current, although recent quantum mechanical treatment[52] has shown that this is not a sufficient mechanism to describe the system.

The experimental configuration is much alike the one illustrated in figure 2.2, where a 10 – 20nm layer of GaAs is grown by molecular beam epitaxy onto a $Al_x\,Ga_{1-x}\,As$ substrate and then covered by another layer of $Al_x\,Ga_{1-x}\,As$, varying from 20nm to 500nm in thickness. The differences in these two semiconductor's conduction and valence bands leads to accumulation layers of both electrons and holes, which are confined to the plane parallel to the interface. This forms the two-dimensional electron gas. The lattice constants of these two semiconductors are almost identical, and there is an absence of unwanted interface states. In some experiments[21–22] an $In_x\,Ga_{1-x}As/GaAs$ heterostructure is used. Sets of interdigital transducers to launch and measure surface acoustic waves are placed upon the surface of the crystal, and in some cases a split gate, positioned perpendicular to the direction of propagation, between the transducers.

## 4.2.2 Areas of Research

### *Acoustoelectric Current*

There is a large amount of literature, both theoretical[19, 27,52] and experimental[23, 27] regarding acoustoelectric current. By applying a negative bias to the gates upon the surface of the crystal, a depletion channel forms within the electron gas, and electrons are transported through the channel in local quantum wells formed by the SAW potential. The geometry of this system can be seen in Fig. 4.3. It was found that in this regime, the acoustoelectric current $I$ versus gate voltage displays a step like behavior. The values of the current on the plateau are quantised[53]:

$$I = n\,e\,f \tag{4.1}$$

where e is the electron charge, $f$ is the SAW frequency and $n$ is the number of electrons transported through the channel per SAW cycle, as also seen in figure 4.3. The remarkably high

accuracy of the quantisation, and high frequency of operation (GHz) suggests possible metrological application, as discussed in chapter one. Interestingly, the quantisation is not observed in the open channel regime,[54] as the mechanism that governs it requires that the DC conductance for each instantaneous configuration of the SAW-induced potential be zero.[55] In the open channel regime this would require channel lengths much longer than the SAW wavelength, which is difficult to realise. As a result the acoustoelectric current displays giant oscillations[54] as a function of gate voltage.

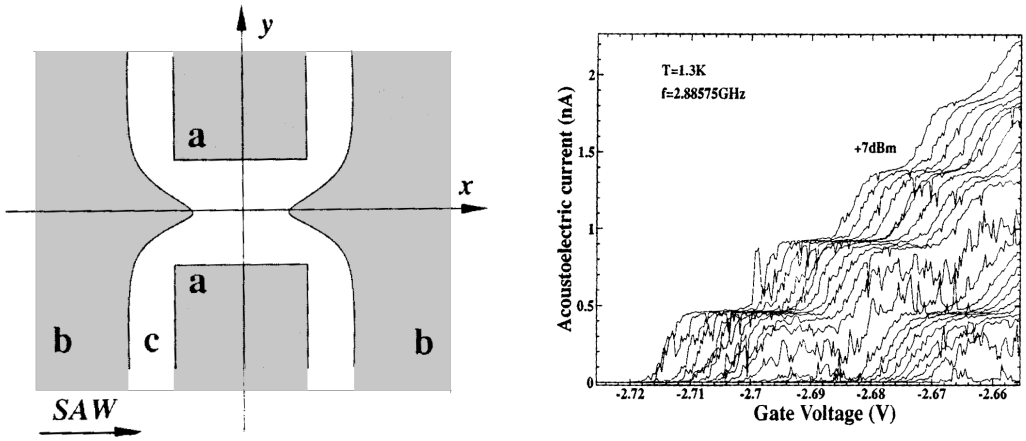


Figure 4.3: (LEFT) Geometry of Acoustoelectric current experiments; (*a*) split gates; (*b*) regions occupied by 2 DEG; (*c*) depleted region. [from Flensberg et al[55]]
(RIGHT) Measured acoustoelectric current vs. gate voltage, for different SAW power levels. [from Talyanskii et al[53]]

Understanding of the nature of the quantisation is the focus of current theoretical research.[52,55] A superposition of the SAW and gate potentials result in the formation of local quantum dots within the channel - and if electrons are captured in these dots they can be transferred through the channel. An increase in SAW power deepens the dots so that more states become available for electrons to occupy, and new plateaus appear. The potential barrier formed by the gates can also be manipulated by changing the gate voltage, which has a similar effect.

As the speed of free electrons is large compared to the velocity of the surface acoustic waves, the electrons are able to follow the changing potential. This means it can be considered as an instantaneous electrostatic problem. To understanding the physics behind this problem, it is important to consider the screening effects and the total contributing effect of potential. The screening length[53] in the 2DEG ($\sim 1\,nm$) is much smaller than the wavelength of the surface wave, $\lambda \sim 10\,\mu m$, so it is assumed that the SAW potential is completely screened in the 2DEG region. Poisson's equation has to be solved subject to the boundary conditions - the potential at

the gates ($\phi = V_g$), in the 2DEG region ($\phi = 0$), and the density $\rho = \rho_o$ of the fixed positive background charge. In addition, the effect of the SAW can be included as a weak periodic modulation of $\rho : \rho \rightarrow \rho_o + \delta\rho(x, t)$. Solving this self-consistently would yield the location of the edge of the 2DEG (which changes in time) and the potential in the depleted region.

The deviations of the current from its quantised value (eqn 5.3) seen in experimental measurements (figure 5.8) is determined primarily by the probability for an electron to tunnel out of the well and return to the electron gas. As the distance between the edge of the 2DEG and the well increases when the SAW propagates through the depleted region, this probability is time dependent. Further corrections to Eqn. 4.1 include nonadiabatic effects near the entrance to the channel at low temperatures[55] and the electrostatic effects between electrons within the dot, known as Coulomb blockade.[19] Investigations into the effects of magnetic fields upon the quantised current have also been made.[25,26]

## *Acousto-optic Effects*

The effects of surface wave propagation on photogenerated carriers in semiconductor heterostructures have become the focus of research in recent years,[21–22] partly due to the availability of state-of-the-art band-gap engineering technology. Particular heterostructures, with desired optoelectronic properties, can be developed to study the dynamics of photogenerated carriers. Strong interband optical transitions are characteristic of semiconductors with very short radiative lifetimes, so traditionally the study of optically excited carriers is experimentally difficult. Initially superlattices, characterised by thin layers of n and p doped semiconductors which extended radiative carrier lifetimes, were grown to study the carriers.

Experimental research[21–22] involving surface wave propagation in $In_{0.15}\,Ga_{0.85}\,As/GaAs$ showed it was possible to extend the radiative lifetime of electron-hole pairs by orders of magnitude. Using interdigital transducers, surface acoustic waves on the (001) plane are propagated along the [110] direction and the light from a pulsed laser diode is used for optical interband excitation above the band gap, and the photoluminescence from recombination is studied using a triple grating spectrometer.

The lateral piezoelectric fields associated with the surface acoustic wave act to separate the electron – hole pairs into the respective adjacent minima and maxima of the conduction and valence bands, modulated by the surface wave potential. The effect of this spatial separation, which is of the order of half a wavelength of the SAW, is an increase in the radiative lifetime. To induce recombination, semitransparent nickel-chromium electrodes are placed a distance away from the excitation site upon the surface of the crystal and screen the lateral piezoelectric fields, and photoluminescence is detected, as seen in Fig. 1.1. The detected photoluminescence increases with increasing acoustic power, until it saturates. This saturation indicates the complete possible occupancy of the wells due the screening effects the dynamic carriers have on the potential.

Another alternative of inducing recombination is the addition of a counter-propagating acoustic wave. If both SAWs have the same wavelength and amplitude, they interfere to create a standing wave. The variation of relative power of these SAWs allows the lifetime and thus location of recombination to be chosen at will. When they differ, electron-hole pairs are trapped and transported in the direction of the most intense surface wave, however, when they are comparable, the standing wave pattern causes an dramatic increase of the overlap of the stored electron-hole pair wavefunctions, which induces recombination. The location of desired recombination can be selected simply by a preset time delay between the surface waves.

The macroscopic distances between excitation and recombination, as well as the ability to select where and when recombination occurs leads to a whole myriad of possible acousto-optic devices. One such example are optical delay lines, which have a significant application[31] as memory elements in optical computer. Others include beam steering and multiplexing/demultiplexing of optical signals on a single chip.

### 4.2.3 Suitable parameters for ACT experiments

The shape of the quantum well associated with the surface acoustic wave varies in width and height depending upon the direction of propagation, as seen in Fig. 4.4. For all known acoustic charge transport experiments, the SAW propagation has always been in the [110] direction on the (001) plane, or equivalent orientations. These directions alone have the highest electromechanical coupling as they are parallel to the polar direction of $\overline{4}$3m cubic crystals, [111].

At present, no results on phonon focusing of $Al_x Ga_{1-x} As$ have been published. It is possible that the concave pure modes may lead to the collective flow of elastic energy in these directions that couples favourably to the piezoelectric fields such that they become comparable in amplitude to those in [110] direction.

The depth at which the GaAs layer is grown is a parameter which is different in many ACT experiments. In most cases it lies close to the surface, where the potential is usually the largest. Although, as was seen in section 3.2.3 the size of the vertical component of the electric field varies quite dramatically over $0.5\,\mu m$. The quantum confined Stark effect (QCSE) occurs when electric fields are perpendicular to quantum wells, and results in the 'tilting' of the conduction and valence bands, and the lowering of energy of bound states. As the wavefunctions are also shifted, this can result in an increase in tunnelling probability. Depending on the thickness of the layer in which the 2DEG lies, the extent of the QCSE would depend on this depth.

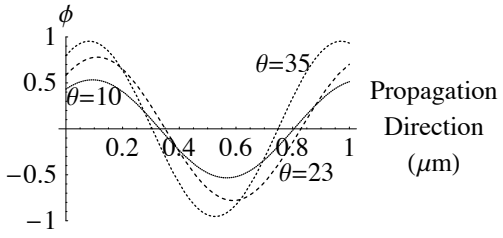


Figure 4.4: The shape of the dynamic quantum well associated with the surface acoustic wave at a depth of 0.14 wavelengths, for three different directions of propagation (in degrees).

Proposed here are two possible propagation directions and a suggested depth for the electron gas. The first propagation direction, [110], is characterised by the highest electromechanical coupling and the second, $\theta = 22.5\,°$, a direction of a concave pure mode. All experiments propagate surface waves in the [110] direction, although the depth that is suggested here does not coincide to those used in experiment.

### *Highest Electromechanical Coupling*

As mentioned previously, the crystallographic direction [110] is parallel to the [111] polar direction. Displacements on the surface are purely longitudinal - so both $A_x$ and $A_y$ components are parallel to [111]. This explains why this two component Raleigh wave experiences the highest piezoelectric coupling.

It is important to compare values quantitatively to the other directions, along the surface wave branch. The boundary conditions for a shorted surface gave a velocity of $2982.36\,m\,s^{-1}$, whilst the free surface velocity was found to be $2983.58 m\,s^{-1}$. This corresponds to an electromechanical coupling constant of 1.142, higher than all values plot in Fig. 3.3. A plot of the SAW potential as a function of depth is depicted in Fig. 4.5.

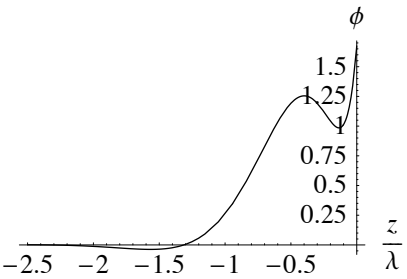


Figure 4.5: The normalised SAW potential for the [110] direction of propagation.

Notice the value of the potential near the surface is greater than all directions show in Fig. 3.6, and it displays Raleigh wave decay as expected. The consequence of this is that the potential well of the SAW will be deeper, and thus more states are available for occupation. This will increase the acoustoelectric current. The chosen depth for this direction is at the bottom of the first well, at $z = -0.14\,\lambda$. The consequences of this depth will be discussed in the next section. The dynamic quantum well associated with the SAW propagating in the 45° direction can be see in Fig. 4.5.

One problem with propagating surface modes in the [110] direction are leaky modes. Orientations of the transducers upon the crystal needs to be exact as the leaky modes attenuate very quickly as the propagation angle moves away from [110]. The interdigital transducers only excite surface modes, so the transverse bulk mode, which has a velocity less than the surface wave mode in this direction, is of no concern.

### *SAW Focusing*

A pure mode of propagation occurs at 22.5°, which is characterised by a locally concave slowness surface. The propagation of surface modes at adjacent angles will contribute to energy flow in the 22.5°direction, and if focusing effects are significant enough, the total contribution may produce a potential in this direction comparable to the potential in the [110] direction.

### *Zero Vertical Piezoelectric Field*

As it was established in section 3.2.3, the vertical component of the piezoelectric field changed dramatically at different depths. The vertical piezoelectric fields in the [110] direction, which for a typical acoustic power are around $10\,\mathrm{kVcm}^{-1}$, alter the potential well that forms the 2DEG. This well has a triangular form, which is discussed in section 4.3.4, and depending upon the polarity of the field, the quantum confined Stark effect can lead to a increase in tunnelling events.

The realisation of this is a decrease in confined charge within the 2DEG. In terms of the quantised acoustoelectric current, this may provide another explanation of the slight slope of the plateaus seen experimental results, although the QCSEs would decrease with increasing gate

voltage. This could also contribute to further explanation of the PL curves in the acousto-optic experiments.

A zero vertical field would ensure that the QCSE would not be present. Based on calculations made in 3.2.3, at the depths at which the electron gas resides in experiments outlined in 4.2.2 would have a non zero piezoelectric field component. Growing a GaAs layer at $0.14\lambda$ below the surface would result in a zero vertical electric field in the [110] direction, and in many directions for small angles from the [100] direction.

The study of exciton ionisation in low dimensional systems[22] would also benefit from zero vertical piezoelectric fields. Measurements of photoluminescence spectra would provide clearer results as there would be no vertical field contributing to the ionisation, and the binding energies attributing to lateral fields could be determined more precisely. The 3D excitons, which have lower binding energies than 2D excitons also need to be taken into consideration, especially as the lateral and vertical piezoelectric fields change with depth.

### 4.3.4 Electron Wavefunction

The experiments conducted by Rocke et al[21–22] involving photogenerated electrons are simplier systems to model than the acoustoelectric current experiments because of the absence of the gate that forms the depletion channel. A simplified model of this problem has two aspects that require consideration - the potential well associated with the surface acoustic wave, and the potential within the layer of semiconductor where the electron gas is formed. The former has sinusoidal form and the approximation[56] for the latter is a triangular well. Suppose the SAW well is assumed to vary in the x-direction, and the 2DEG well in the z-direction. To find the wavefunctions $\psi$(x,z) and associated energies $\mathcal{E}$ of a single electron in these potentials, consider the time independent two dimensional Schrödinger equation

$$\left(-\frac{\hbar^2}{2m}\nabla^2 + (V_X + V_Z)\right)\psi(x, z) = \mathcal{E}\,\psi(x, z) \tag{4.2}$$

The wavefunctions can be separated such that

$$\left(-\frac{\hbar^2}{2m}\partial_x{}^2 + V_X\right)X(x) = \mathcal{E}_x\,X(x) \qquad \text{and} \qquad \left(-\frac{\hbar^2}{2m}\partial_z{}^2 + V_Z\right)Z(z) = \mathcal{E}_z\,Z(z) \tag{4.3}$$

where

$$\psi(x, z) = X(x)\,Z(z) \tag{4.4}$$

*Solution for the SAW potential*

The potential in the x-direction is shown in Fig. 4.6, which has the form

$$V(x) = \phi_d \cos\left(\frac{2\pi x}{\lambda}\right) \tag{4.5}$$

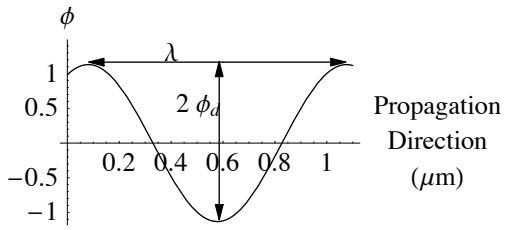


Figure 4.6: The quantum well associated with the SAW potential

The Schrödinger equation is

$$\left(-\frac{\hbar^2}{2m}\frac{d^2}{dx^2} + \phi_d \cos\left(\frac{2\pi x}{\lambda}\right)\right)\psi(x) = \mathcal{E}\,\psi(x) \tag{4.6}$$

The solution to this represents the wavefunction of an electron in a periodic potential. It is useful to redefine this equation into a form know as the Mathieu equation[56]

$$\psi''(s) + (\alpha - 2q\cos(2s))\,\psi(s) = 0 \tag{4.7}$$

with energy parameter, $\alpha$, and potential amplitude, q;

$$s = \frac{\pi x}{\lambda} \qquad \alpha = \frac{2m\lambda^2\,\mathcal{E}}{\pi^2\,\hbar^2} \qquad q = \frac{m\lambda^2\,\phi_d}{\pi^2\,\hbar^2} \tag{4.8}$$

In order to establish solutions of the Mathieu equation, first consider the case of zero potential, $q = 0$. The unnormalised standing wave solutions are

$$\psi(s) = \cos(m\,s),\ \sin(m\,s)$$
$$\alpha = m^2;\ \ m = 1, 2, 3, \ldots$$

When $q \neq 0$, the energy parameter and wave function will both depend on q, and these can both be expressed by power series:

$$\alpha_m(q) = m^2 + \sum_{n=1}^{\infty} \alpha_n \, q^n$$

$$\psi_m(s, q) = \cos(m\,s) + \sum_{n=1}^{\infty} c_n(s)\, q^n \qquad \text{or} \qquad \psi_m(s) = \sin(m\,s) + \sum_{n=1}^{\infty} s_n(s)\, q^n \tag{4.9}$$

These wave functions are known as the cosine and sine elliptic functions[56], and are well know in other physical problems involving elliptic shapes or periodic potentials. The wave function coefficients $c_n(s)$ and the energy cooefficients $\alpha_n$ are found by substituting the expressions (Eqns 4.9) back into the Matheiu equation (Eqn 4.7), for a particular value of m, and equating powers of q. The resulting equations are solved by using symmetry conditions and successive integrations. Hence $\alpha_m(q)$ and $\psi_m(s,q)$ can be found to any desired accuracy. In terms of the original variables, the energy and unnormalised wavefunction for an electron in the SAW potential well are given as

$$\mathcal{E}_m = \frac{\hbar^2\,\pi^2}{2\,m\,\lambda^2}\left(m^2 + \sum_{n=1}^{\infty} \alpha_n \left(\frac{m\,\lambda^2\,\phi_d}{\pi^2\,\hbar^2}\right)^n\right) \tag{4.10}$$

$$\psi_m(x) = \cos\left(\frac{m\,\pi\,x}{\lambda}\right) + \sum_{n=1}^{\infty} c_n\left(\frac{\pi\,x}{\lambda}\right)\left(\frac{m\,\lambda^2\,\phi_d}{\pi^2\,\hbar^2}\right)^n \tag{4.11}$$

### *Solution for 2DEG potential*

For the case of the layer within the semiconductor heterostructure, using the triangular well approximation[57], the potential is given as

$$V(z) = e\,F\,z$$

where $-e\,F$ is the corresponding electric field. The Schrödinger equation looks like

$$\left(-\frac{\hbar^2}{2\,m}\,\frac{d^2}{dz^2} + e\,F\,z\right)\psi(z) = \mathcal{E}\,\psi(z) \tag{4.12}$$

The triangular well approximation is characterised by an infinite step on one side of the well. No electrons can exist beyond this, so the boundary condition is

$$\psi(0) = 0$$

It is useful to express Eqn. 4.12 in a different form

$$\frac{d^2\psi(\bar{z})}{d\bar{z}^2} = (\bar{z} - \bar{\mathcal{E}})\,\psi(\bar{z}) \tag{4.13}$$

where

$$\bar{z} = \frac{z}{z_o} \qquad \bar{\mathcal{E}} = \frac{\mathcal{E}}{\mathcal{E}_o} \qquad z_o = \left(\frac{\hbar^2}{2\,m\,e\,F}\right)^{\frac{1}{3}} \qquad \mathcal{E}_o = \left(\frac{e\,F\,\hbar}{2\,m}\right)^{\frac{1}{3}} = e\,F\,z_o$$

By defining a new variable, s;

$$s = \bar{z} - \bar{\mathcal{E}}$$

Now Eqn. 4.13 reduces to the familiar Airy-Stokes equation

$$\frac{d^2\psi(s)}{d\,s^2} = s\,\psi(s)$$

The solutions of this equation are known as Airy functions, Ai(s) and Bi(s). The second Airy function Bi(s) is unbounded for $s \to \infty$, so it is rejected. The boundary condition is

$$\mathrm{Ai}(-\bar{\mathcal{E}}) = 0$$

Notice that the zeros of the Airy function, which satisfy the boundary condition, correspond to the eigenvalues of Eqn. 4.13 which are the rescaled energies of this system. All of the zeros of Ai(s) are negative, so defining the $n^{\text{th}}$ zero $a_n = -c_n$ the allowed energies are given by:

$$\mathcal{E}_n = c_n\left[\frac{(e\,F\,\hbar)^2}{2\,m}\right]^{\frac{1}{3}} \qquad n = 1, 2, 3, \ldots.$$

The roots $c_n$ can be approximated using WKB theory[57]

$$c_n \simeq \left[\frac{3\,\pi}{2}\left(n - \frac{1}{4}\right)\right]^{\frac{2}{3}}$$

The unnormalised wavefunctions are

$$\psi_n(z) = \mathrm{Ai}(s_n) = \mathrm{Ai}(\bar{z} - \bar{\mathcal{E}}_n) = \mathrm{Ai}\left(\frac{e\,F\,z - \mathcal{E}_n}{\mathcal{E}_o}\right)$$

Now considering the problem in two dimensions, the total energy of the ground state can be calculated, given a potential $\phi_d$ and SAW wavelength $\lambda$:

$$\mathcal{E}_{1,1} = \frac{\hbar^2\,\pi^2}{2\,m\,\lambda^2}\left(1^2 + \sum_{p=1}^{\infty}\alpha_p\left(\frac{m\,\lambda^2\,\phi_d}{\pi^2\,\hbar^2}\right)^p\right) + 2.338\left(\frac{(e\,F\,\hbar)^2}{2\,m}\right)^{\frac{1}{3}} \tag{4.14}$$

The full wavefunction, $\psi_{n,m}(x, z)$, with normalisation constant $\zeta_{n,m}$, will look like

$$\psi_{n,m}(x, z) = \zeta_{n,m}\,\mathrm{Ai}\left(\frac{e\,F\,z - \mathcal{E}_n}{\mathcal{E}_o}\right)\left(\cos\left(\frac{m\,\pi\,x}{\lambda}\right) + \sum_{p=1}^{\infty} c_p\left(\frac{\pi\,x}{\lambda}\right)\left(\frac{m\,\lambda^2\,\phi_d}{\pi^2\,\hbar^2}\right)^p\right)$$

This would be a valid approximation of the wavefunction for an electron within the two dimensional electron gas through which a continous piezoelectric surface acoustic wave is travelling.

# Chapter Five: Summary

## 5.1 Conclusions

### 5.1.1 Surface Acoustic Waves

A superposition of four plane waves formed the surface wave solution of the piezoelectric elastic wave equation for the (001) surface of $Al_{0.3}$ $Ga_{0.7}$ As. These solutions satisfied the stress-free boundary conditions associated with a free surface and the requirement that the amplitudes of displacement vanish at a finite depths.

The wave equations and boundary conditions simplify in the high symmetry directions, and surface wave solutions for cubic crystals in these directions have been treated in many publications. However, there is limited literature on propagation in arbitrary directions in piezoelectric cubic crystals, and none could be found for $Al_x$ $Ga_{1-x}$As. The propagation directions between [100] and [110], which covers all unique directions for the (001) plane, were studied numerically. Compared to the non-piezoelectric surface wave solutions, the amplitude corresponding to the additional term when piezoelectric coupling is included is insignificant - at most only contributing to 2% of the total potential.

The outstanding feature of these surface modes was the oscillatory decay into the bulk, which was a direct consequence of the complex decay constant. These solutions are commonly known as Rayleigh waves. Solving for the roots of the boundary condition matrix determinant yielded the allowed velocities of the surface wave. These velocity results showed two important features – the degeneration of the surface wave mode for $\theta > 30°$ into a bulk mode at [110] which satisfies the stress-free boundary conditions; and the presence of leaky surface modes for $\theta > 25°$at velocities above the lowest bulk wave velocity. These leaky modes are characterised by small imaginary components in the wavevector parallel to the surface, and a positive imaginary component of one of the decay constants. These leaky modes attenuate in the direction of propagation and leak energy away from the surface into the bulk of the material.

The displacements of the surface acoustic wave changed dramatically as the propagation direction changed. At [100] the wave is elliptically polarised in the sagittal plane, and as $\theta$ increases the longitudinal and vertical components become smaller and a transverse component appears. By the time the propagation is directed in the [110] direction, the longitudinal and vertical components have vanished and the surface modes became degenerate with the single bulk transverse mode. Alternatively, following the leaky branch to the [110] direction, the longitudinal and vertical polarisation increase as the transverse component begins to decrease and completely

vanishes for the surface wave solution at [110] whose displacements are polarised in the sagittal plane.

### 5.1.2 Piezoelectric Potential and Energy Flow

The piezoelectric fields and potential play a significant role in acoustic charge transport phenomena and display some interesting features as a result of the anisotropy of $Al_{0.3}$ $Ga_{0.7}$ As. From a crystallographic point of view, piezoelectric fields result from strains in the polar direction of the $\overline{4}$3m point group - the [111] direction. The consequence of this on the (001) plane is that longitudinal strain in the [110] direction will result in the highest piezoelectric coupling.

Two main aspects of the electric potential were considered: how it varied with propagation direction, and how it varied with depth. The plots of this potential against propagation direction indicated that for depths $z \gtrsim -0.25\,\lambda$, the potential was relatively larger over the regions closer to the [110] direction (ie $\theta \gtrsim 22.5°$), and only marginally smaller for depths $z \lesssim 0.25\,\lambda$ for directions closer to [100]. The decay into the bulk of the potential provide an explanation for this, as the profile in the $z-$direction changes quite significant for different propagation directions. The highest value for the potential was found for the surface wave mode at [110].

The piezoelectric fields associated with the surface acoustic wave also varied significantly over the range of propagation directions. The longitudinal fields were shown to have a behave similar to the potential, as expected. The potential has a wave-like dependence, and is invariant in the transverse direction. The resulting transverse electric field is zero, for all directions of propagation. The vertical electric field displayed some very interesting features for a range of different depths and directions. At angles close to the [100] direction, for a depth $z \simeq 0.14\,\lambda$ there was a zero vertical field. The potential profile as a function of depth explained this - showing a well structure close to the surface - and the depth at the centre of this well would give a zero vertical field.

The focusing effects were investigated using two methods, first the analysis of the direction of the a power flow vector $\mathbf{W}$ and the wavevector $\boldsymbol{k}_{\|}$, and then a more qualative method - slowness surfaces. The slowness surface relied purely upon the phase velocity, whereas the power flow vector depended on all SAW characteristics. Both yielded the same results. Pure mode directions for $0 < \theta < 90°$ were found in the high symmetry directions [100], [110], [010] as well as two concave pure modes at ~22.5° and ~67.5°. The group velocities of surface acoustic waves propagating adjacent direction will point in the same direction, and energy will be focussed in this direction.

### 5.1.3 Acoustic Charge Transport

All acoustic charge transport experiments propagate surface waves in the [110] direction of the (001) plane (or equivalent directions) on a GaAs based heterostructure. Free carriers within the two dimensional gas are trapped within the minima of the piezoelectric potential associated with the travelling surface wave. In the presence of a negatively biased gate on the surface of the crystal, a depletion layer is formed with the 2DEG, and the charge transport is quantised. This is known as the acoustoelectric current, which is of the order of nanoamps. The full mechanism of this quantised current is not yet understood, and the possible metrological applications as a current standard has seen research intensify into this aspect of acoustic charge transport.

For experiments investigating the acoustoelectric current, the depth at which the GaAs layer is grown ranges between 100-500nm. It would be worth investigating the nature of the current on a heterostructure with a 2DEG at a depth of $z = -0.14\,\lambda$ (~140nm for a SAW wavelength of 1$\mu$m). In this case there is an absence of vertical piezoelectric fields, and as a result an absence of the quantum confined Stark effect. This could provide more accurate measurements of the current, and the effect of vertical piezoelectric fields could be determined.

If focusing effects are significant, propagation in the $\theta = 22.5\,°$ direction could yield a piezoelec tric potential comparable or even greater than that in [110]. The greater the potential the larger the occupancy of the well and the greater the current. Although the [110] direction provides the highest electromechanical coupling, the presence of highly attenuated leaky modes on each direction immediately adjacent of this direction requires precise engineering of the interdigital transducers upon the heterostructure.

## 5.2 Future Research

The next fundamental step in the surface acoustic wave problem is to consider the dynamical response of the system by solving the wave equation subject to a driving term. There are a number of mathematical techniques that can be used, although the obvious choice is a Green's functions method. Once the nine (or in the piezoelectric case, 16) Green's tensor elements have been found, the response of the system to an arbitrary driving force can be determined. Real values can then be determined for the amplitudes, piezoelectric fields and potentials for a specific acoustic power.

Studies can then be turned to the phonon focusing aspect on $Al_{0.3}\,Ga_{0.7}\,As$, and a quantitative analysis can be made. Focusing patterns can be developed, and the strength of focusing in particular directions can be determined. A consequence might be that channels would be formed by the SAWs and the gates used in previous experiments may not be necessary.

There is a myriad of acoustic charge transport related research to consider. One interesting application is the effect of a point source of acoustic waves on a surrounding electron gas. In this system the effects of phonon focusing will be of prime consideration.

Exciton ionisation in the well still has yet to be fully understood. The transition process between the bound states of the moving well and the ionised electron-hole pairs requires consideration, and the experiment described previously would be an excellent tool to study these excitons. As the lateral and vertical piezoelectric fields vary with direction, by optically exciting carriers at a central location on the crystal and driving the point source, deliberate screening at radial locations on the sample will result in a detected photoluminescence due to recombination. Taking into account the propagation directions for each of these spectra, binding energies of 2D and 3D excitons can be calculated, and further insight into the mechanism of the transition can be made.

# References


[1] Lord Rayleigh, London Math. Soc. Proc. **17**, 4 (1887).
[2] R. Stoneley, R., Proc. R. Soc. London, Ser A **232**, 447 (1955).
[3] J. L. Synge, J. Math. Phys. **35**, 323 (1957).
[4] D. C. Gazis, R. Herman, R. F. Wallis, Phys. Rev. **119**, 533 (1960).
[5] V. T. Buchwald, A. Davis, Nature **191**, 899 (1961).
[6] D. A. Tursonov, Soviet. Phys. Acoust. **13**, 78 (1967).
[7] G. W. Farnell: "Properties of Elastic Surface Waves", in *Physical Acoustics*, Vol. 6, edited by W. P. Mason, R. N. Thurston (Academic, New York, 1970).
[8] I. A. Viktorov, *Rayleigh and Love Waves*, Section 1.1 (Plenum, New York, 1967).
[9] J. E. May, IEEE Spectrum **2**, 73 (1965).
[10] R. M. White, F. W. Voltmer, Appl. Phys. Lett. **7**, 314 (1965).
[11] C.-C. Tseng, J. Appl. Phys. **38**, 4281 (1967).
[12] C.-C. Tseng, J. Appl. Phys. **41**, 2270 (1970).
[13] R. M. White, IEEE Trans. Elect. Dev. **ED14**, 181 (1967).
[14] H. F. Tiersten, J. Appl. Phys. **40**, 770 (1969).
[15] D. L. White, IEEE Ultrasonics Symp., Vancouver (1967).
[16] E. Stern, Lincoln Lab. Tech. Note No. 1968-36, M.I.T. (1968).
[17] S. H. Simon, Phys. Rev. B **54**, 13878 (1996).
[18] G. Gumbs, G. R. Aizin, M. Pepper, Phys. Rev. B **57**, 1654 (1998).
[19] G. Gumbs, G. R. Aizin, M. Pepper, Phys. Rev. B **60**, 13954 (1999).
[20] G. R. Aizin, G. Gumbs, M. Pepper, Phys. Rev. B **58**, 10589 (1998).
[21] C. Rocke, S. Zimmermann, A. Wixforth, J. P. Kotthaus, G. Bohm, G. Wiemann, Phys. Rev. Lett. **78**, 4099 (1997).
[22] C. Rocke, A. O. Govorov, A. Wixforth, G. Bohm, G. Weimann, Phys. Rev. B **57**, R6850 (1998).
[23] J. Cunningham, V. I Talyanskii, J. M. Shilton, M. Pepper, M. Y. Simmons, D. A. Ritchie, Phys. Rev. B **60**, 4850 (1999).
[24] Y. Levinson, O. Entin-Wohlman, R. Wolfle, Phys. Rev. Lett. **85**, 634 (2000).
[25] V. I. Falko, S. V. Meshkov, S. V. Iordanskii, Phys. Rev. **47**, 9910 (1993).
[26] A. L. Efros, Y. M. Galperin, Phys. Rev. Lett. **64**, 1959 (1990).
[27] A. O. Govorov, A. V. Kalameitsev, M. Rotter, A. Wixforth, J. P. Kotthaus, K.-H. Hoffmann, N. Botkin, Phys. Rev. B **62**, 2659 (2000).
[28] J. Cunningham, V. I. Talyanskii, J. M. Shilton, M. Pepper, A. Kristensen, P. E. Lindelof, Phys. Rev. B **62**, 1564 (2000).
[29] M. W. Keller, J. M. Martinis, N. M. Zimmerman, A. H. Steinbach, Appl. Phys. Lett. **69**, 1804 (1996).

[30] T. J. Thornton, M. Pepper, H. Ahmed, D. Andrews, G. J. Davies, Phys. Rev. Lett. **56**, 1198 (1986).
[31] R. Matthews, New Scientist **162**, No. 2189, pp28-32.
[32] C. H. W. Barnes, J. M. Shilton, A. M. Robinson, Phys. Rev. B **62,** 8410 (2000).
[33] E. Dieulesaint, D. Royer, *Elastic Waves in Solids* (Wiley, Chichester, 1980).
[34] S. Wang, *Solid-State Electronics* (McGraw-Hill, New York, 1966).
[35] A. A. Oliner, *Acoustic Surface Waves* (Springer, Berlin, 1978).
[36] J. Sapriel, J. C. Michel, J. C. Toledano, R. Vacher, J. Kervarec, A. Regreny, Phys. Rev. B **28**, 2007 (1983).
[37] V. E. Steel, W. D. Hunt, M. A. Emanuel, J.J. Coleman, J. Appl. Phys. **66**, 90 (1989).
[38] R. W. Keyes, J. Appl. Phys. **33**, 3371 (1962).
[39] S. Adachi, J. Appl. Phys. **58**, R1 (1985).
[40] S. Adachi, *GaAs and Related Materials* (World Scientific, Singapore, 1994).
[41] W. D. Hunt, R. L. Miller, B. J. Hunsinger, J. Appl. Phys. **60**, 3532 (1986).
[42] G. Arlt, P. Quadflieg, Phys. Status Solidi **25**, 323 (1968).
[43] K. Hubner, Phys. Statues Solidi B **57**, 627 (1973).
[44] E. D. Palik, *Handbook of Optical Constants of Solids* (Academic, Boston, 1985).
[45] J. J. Campbell, W. R. Jones, IEEE Trans. Sonics. Ultrasonics **SU15**, 209 (1968).
[46] F. Rosch, O. Weis, Z. Phys. B **25**, 115, (1976).
[47] G. A. Northrop, Phys. Rev. B **26**, 903 (1982).
[48] R. E. Camley, A. A. Maradudin, Phys. Rev. B **27**, 1959 (1983).
[49] H. Shirasaki, T. Makimoto, J. Appl. Phys. **49**, 658 (1978).
[50] H. Shirasaki, T. Makimoto, J. Appl. Phys. **50**, 2795 (1979).
[51] R. L. Stamps, R. E. Camley, Phys. Rev. B **31**, 4924 (1985).
[52] Y. Levinson, O. Entin-Wohlman, P. Wolfle, Phys. Rev. Lett. **85**, 634, (2000).
[53] V. I. Talyanskii, J. M. Shilton, M. Pepper, C. G. Smith, C. J. B. Ford, E. H. Linfield, D. A. Ritchie, G. A. C. Jones, Phys. Rev. B **56**, 15180, (1997).
[54] H. Totland, Yu. M. Galperin, Phys. Rev. Lett. **54**, 8814, (1996).
[55] K. Flensberg, Q. Niu, M. Pustilnik, Phys. Rev. B **60**, R16291, (2000).
[56] S. G. Davison, M. Steslicka, *Basic Theory of Surface States* (Oxford, New York, 1996)
[57] J. H. Davies, *The Physics of Low-Dimensional Semiconductors* (Cambridge, Cambridge, 1998)